Biophysical *Journal*
Article

Biophysical Society

The structural basis of BCR-ABL recruitment of GRB2 in chronic myelogenous leukemia

Yonglan Liu,[1] Hyunbum Jang,[2] Mingzhen Zhang,[2] Chung-Jung Tsai,[2] Ryan Maloney,[1] and Ruth Nussinov[2,3,*]
[1]Cancer Innovation Laboratory, National Cancer Institute, Frederick, Maryland; [2]Computational Structural Biology Section, Frederick National Laboratory for Cancer Research, Frederick, Maryland; and [3]Department of Human Molecular Genetics and Biochemistry, Sackler School of Medicine, Tel Aviv University, Tel Aviv, Israel

ABSTRACT BCR-ABL drives chronic myeloid leukemia (CML). BCR binding to GRB2 transduces signaling via the Ras/MAPK pathway. Despite considerable data confirming the binding, molecular-level understanding of exactly how the two proteins interact, and, especially, what are the determinants of the specificity of the $SH2^{GRB2}$ domain-phosphorylated BCR (pBCR) recognition are still open questions. Yet, this is vastly important for understanding binding selectivity, and for predicting the phosphorylated receptors, or peptides, that are likely to bind. Here, we uncover these determinants and ascertain to what extent they relate to the affinity of the interaction. Toward this end, we modeled the complexes of the pBCR and $SH2^{GRB2}$ and other pY/Y-peptide-SH2 complexes and compared their specificity and affinity. We observed that pBCR's $_{176}$FpYVNV$_{180}$ motif is favorable and specific to $SH2^{GRB2}$, similar to pEGFR, but not other complexes. $SH2^{GRB2}$ contains two binding pockets: pY-binding recognition pocket triggers binding, and the specificity pocket whose interaction is governed by N179 in pBCR and W121 in $SH2^{GRB2}$. Our proposed motif with optimal affinity to $SH2^{GRB2}$ is E/D-pY-E/V-N-I/L. Collectively, we provide the structural basis of BCR-ABL recruitment of GRB2, outline its specificity hallmarks, and delineate a blueprint for prediction of BCR-binding scaffolds and for therapeutic peptide design.

SIGNIFICANCE BCR-ABL fusion protein, encoded by the Philadelphia chromosome, drives chronic myeloid leukemia (CML). BCR is a GTP exchange factor controlling small GTPases. ABL is a kinase. BCR binding to GRB2 adaptor protein transduces the oncogenic signal. Despite considerable data confirming the binding, molecular-level understanding of exactly how the two proteins interact, and, especially, what are the determinants of the specificity of the recognition are still open questions. Yet, this is vastly important for binding selectivity, and for predicting the phosphorylated receptors, or peptides, that are likely to bind. This work uncovers the structural basis for the specific BCR-ABL-GRB2 binding, maps a blueprint to predict signal transducers to bypass targeted BCR-ABL–GRB2 in drug resistance, and delineates key attributes in inhibitor design.

INTRODUCTION

The translocation of the so-called Philadelphia chromosomes between chromosome 22, containing a breakpoint cluster region (BCR) sequence, and chromosome 9, containing an Abelson protooncogene (ABL) sequence, generates the *BCR-ABL* fusion gene (Fig. 1 *a*) (1–3). *BCR-ABL* encodes a cytoplasmic BCR-ABL oncoprotein with constitutively enhanced and dysregulated tyrosine kinase activity that disrupts key cellular processes (4,5). Different breakpoints of the BCR protein in the translocation result in different forms of the BCR-ABL protein (Fig. 1 *b*). These are p190, p210, and p230 BCR-ABL, which are associated with acute lymphoblastic leukemia, chronic myeloid leukemia (CML), and neutrophilic-CML, respectively (6). CML is a malignancy originating from hematopoietic stem cells. The disease involves three stages, chronic phase, accelerated phase, and blast crisis, featured by different amounts of blasts, peripheral white blood cells, and bone marrow cells (6–8). CML-related chimeric p210 BCR-ABL oncoprotein impacts multiple cell signaling pathways, driving CML pathogenesis (6,9–11).

Ras/mitogen-activated protein kinase (MAPK) is a key pathway controlling cell proliferation and its hyperactivation is responsible for malignant transformation in cancer. Different cell lines and murine models show that BCR-ABL elevates Ras activity, which promotes the transformation of

Submitted January 21, 2022, and accepted for publication May 20, 2022.
*Correspondence: NussinoR@mail.nih.gov
Editor: Elizabeth Rhoades.
https://doi.org/10.1016/j.bpj.2022.05.030

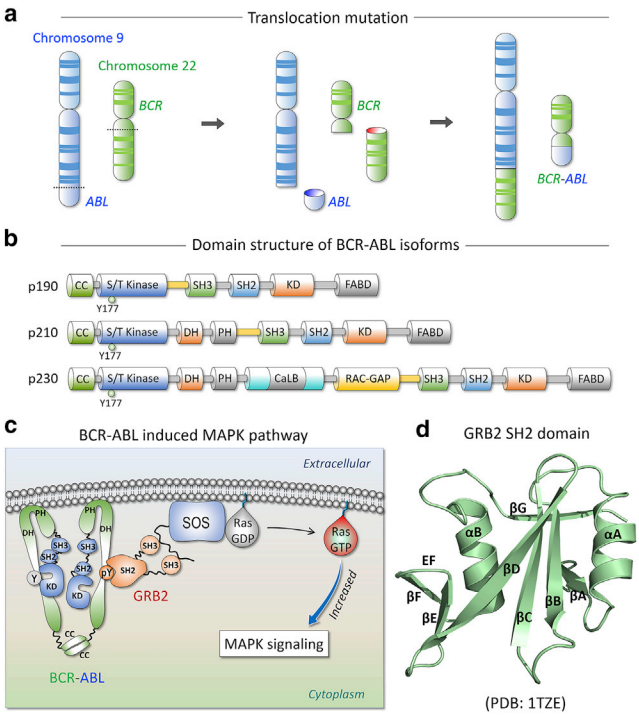

FIGURE 1 (*a*) Translocation mutation between chromosome 9 and chromosome 22. Chromosome 9 and chromosome 22 contain the *ABL* and *BCR* genes, respectively. Upon translocation, the two genes are fused together and form the *BCR-ABL* gene. (*b*) Domain organization of three isoforms of BCR-ABL oncoprotein, p190, p210, and p230 BCR-ABL. The three isoforms contain different lengths of BCR sequences but have the same ABL sequence. BCR contains a coiled-coil (CC) domain, a serine/threonine (S/T) kinase domain, a Dbl homology (DH) domain, a pleckstrin homology (PH) domain, a putative calcium-dependent lipid-binding site (CaLB), and a RAC guanosine triphosphatase-activating protein (RAC-GAP) domain. ABL has an SH3 domain, an SH2 domain, a kinase domain (KD), and an F-actin-binding domain (FABD). (*c*) Schematic illustration of BCR-ABL recruitment of GRB2 in the activation of Ras. (*d*) Crystal structure of GRB2 SH2 domain (PDB: 1TZE).

fibroblasts, hematopoietic cells, and murine bone marrow (12). BCR-ABL-associated Ras signaling can be mediated by cytoplasmic adaptor proteins (13), primarily growth factor bound protein 2 (GRB2), and Src homology 2 (SH2) domain protein C1 (SHC), with BCR-ABL recruiting GRB2/Son of sevenless (SOS) complex (12). The resulting BCR-ABL/GRB2/SOS assembly stimulates the transformation of inactive GDP-bound state of Ras to its active GTP-bound form (Fig. 1 *c*) (6,14,15), in turn constitutively promoting Raf/mitogen-activated protein kinase kinase/extracellular signal-regulated kinase signaling. In leukemia, the gene encoding GRB2 is frequently duplicated, leading to its overexpression (16,17), increasing the number of BCR-ABL/GRB2/SOS complexes, and escalating Ras activation, thus causing a proliferation of hemopoietic cells and CML oncogenesis (12). Disruption of GRB2/SOS complexes through ablation of GRB2 nSH3 and cSH3 domains (18) or by high-affinity GRB2-binding peptides (19) decreases BCR-ABL-induced cell proliferation. GRB2 SH3-deletion mutants are unable to bind SOS and can reverse BCR-ABL-induced cell proliferation (18). In human hematopoietic cells, reduced GRB2 expression can inhibit both BCR-ABL-GRB2 and GRB2-SOS interactions, significantly reducing the proliferation and survival of CD34+ cells (20). These observations emphasize the essential role of GRB2 in CML, which links BCR-ABL to Ras signal transduction. Here, overactivation of ABL in the cytoplasm upon binding to BCR is seen as the main mechanism by which CML progresses. Nonetheless, even though the phosphorylated BCR (hereafter refers to pBCR) in complex with GRB2 plays a key role in activation of Ras, other pathways, such as Ras/MAPK, phosphoinositide 3-kinase (PI3K)/protein kinase B (AKT), Janus kinase/signal transducer and activator of transcription, stress-activated protein kinase/c-Jun N-terminal kinase, nuclear factor κB, and c-Myc can also be engaged (12). This is particularly important since blocking the Ras activation, may promote drug resistance in ABL overactivation through these pathways.

The first exon region of the p210 BCR protein contains the phosphorylation site for GRB2 binding, which is required for inducing CML (12). Different lengths of BCR sequences fused into ABL protein result in different leukemia types, which depend on the precise breakpoints in the translocation and RNA splicing. p210 contains multiple domains for cell signal transduction, including a coiled-coil domain, a serine/threonine kinase domain, a Dbl homology domain, and a pleckstrin homology domain. Tyrosine at position 177 (Y177) in the BCR serine/threonine domain is the binding site for GRB2 (Fig. 1, *b* and *c*). Phosphorylated Y177 (pY177) stimulates GRB2 recognition through the SH2 domain interaction. Y177F substitution diminishes GRB2 binding to BCR-ABL in vivo and abolishes BCR-ABL-induced Ras signal transduction, reducing cell proliferation in murine and human myeloid progenitor (21–23). These observations validate the BCR-ABL-GRB2 interaction as indispensable for CML induction.

GRB2 is an adaptor protein (24,25). It contains a conformationally conserved SH2 domain (hereafter referred to as $SH2^{GRB2}$) flanked by N-terminal and C-terminal SH3 domains (nSH3 and cSH3) (Fig. 1 *c*) (25–32). Both SH3 domains recruit the proline-rich, C-terminal tail of SOS1 containing the PXXP motif (X represents any natural amino acid), while its SH2 domain recognizes and binds with high affinity a specific phosphorylated tyrosine in the pYXN motif (33) of receptor tyrosine kinases (34), such as platelet-derived growth factor (PDGF), insulin receptor substrate 1 (35), and epidermal growth factor receptor (EGFR) (36,37), and other signaling proteins, such as BCR (38), SHC (35), and SH2 domain-containing phosphatase 2 (39). The SH2 domain can recognize these proteins as long as the tyrosine in the motifs is phosphorylated, leading to the release of the GRB2 nSH3 and cSH3 "arms" (40,41). The liberated GRB2 SH3 domains recruit and relocate SOS1 by interacting with its proline-rich region for membrane association (42). $SH2^{GRB2}$ is responsible for the binding with BCR-ABL, underscoring the importance and potential usefulness of in-depth understanding of the

structural details of the interaction. $SH2^{GRB2}$ contains ~100 amino acids. It presents a globular module with three β-strands forming an antiparallel β-sheet in the central core flanked by α-helices on both sides (Fig. 1 *d*). Although there is a crystal structure of $SH2^{GRB2}$ in complex with the pBCR peptide containing pY177, key questions exist. The crystal structure presents a seven-residue sequence of $_{174}$KPFpYVNV$_{180}$ bound to $SH2^{GRB2}$ (Fig. S1). However, the crystal structure cannot capture the dynamic interactions between the ligand and the receptor, which may overlook important contextual interaction information. In healthy cells, in the presence of an upstream signal, phosphorylated EGFR (hereafter refers to pEGFR) recruits GRB2 through the SH2 interaction activating the Ras/MAPK pathway (43–45). However, in CML cells, in the absence of a receptor tyrosine kinase signal, BCR-ABL activates the Ras/MAPK pathway, leading to aberrant cell proliferation in CML.

Here, we performed molecular modeling and molecular dynamics (MD) simulations to obtain the structural basis for the interaction between BCR-ABL and $SH2^{GRB2}$ at the atomic level. The pBCR, BCR, pEGFR, and EGFR peptides in complex with $SH2^{GRB2}$ were modeled and the interactions between the peptides and the SH2 domains were investigated. p85α is the regulatory subunit of PI3Kα. The PI3Kα/AKT/mTOR pathway is vital for cell growth, which is required for cell proliferation (46). p85α contains the nSH2 and cSH2 domains that recognize pY-peptides containing the pYXM motif (47). We thus added models of pBCR and BCR with the nSH2 and cSH2 domains of p85α for comparison. Our collective simulation results showed that pBCR favorably and specifically binds to $SH2^{GRB2}$. This binding is similar to that of pEGFR-$SH2^{GRB2}$. However, pBCR shows unspecific binding to $nSH2^{p85\alpha}$ and unfavorable binding to $cSH2^{p85\alpha}$. We observed that the five-residue sequence of FpYVNV is the preferred binding motif of $SH2^{GRB2}$. Tyrosine phosphorylation triggers the binding through strong interactions in the pY-binding pocket. When pBCR is stably bound to $SH2^{GRB2}$, the motif adopts a type I β-turn conformation, mainly induced by the interaction in the specificity pocket, whose organization is conformationally selected by $SH2^{GRB2}$. We demonstrate that the specific interaction in this pocket requires the bilateral factors of the Asn residue at the +2 position C-terminal to pY in the binding motif and W121 in the EF loop of GRB2 SH2 domain. Importantly, residues near pY and Asn influence the binding affinity, which explains why BCR-ABL can inhibit EGFR binding to $SH2^{GRB2}$. This couples with the higher GRB2 population due to gene duplication. Our analysis of the affinities of different binding motifs to $SH2^{GRB2}$, in combination with precise residue-residue interactions between the peptide ligand and $SH2^{GRB2}$ in our simulation, lead us to propose the optimal binding motif for $SH2^{GRB2}$. Altogether, here we map the detailed hallmarks of the interaction, which can be exploited for prediction of other GRB2 receptor partners or candidate scaffolds that BCR can bind in CML drug resistance and provide a blueprint for a therapeutic high-specificity and high-affinity peptide inhibitor design.

MATERIALS AND METHODS

Modeling of pY-peptide-SH2 and Y-peptide-SH2 complexes

The initial configurations of pY-peptide-SH2 and Y-peptide-SH2 complexes were derived from crystal structures (PDB: 1TZE for pBCR-$SH2^{GRB2}$ and BCR-$SH2^{GRB2}$; PDB: 1ZFP for pEGFR-$SH2^{GRB2}$ and EGFR-$SH2^{GRB2}$; PDB: 2IUI for pBCR-$nSH2^{p85\alpha}$ and BCR-$nSH2^{p85\alpha}$; PDB: 1H9O for pBCR-$cSH2^{p85\alpha}$ and BCR-$cSH2^{p85\alpha}$) (Table 1). To capture the interaction information between the peptides and the SH2 domains as more as possible, the shorter sequences of the peptides in the crystal structures were extended to 17-amino acid-long peptides ($_{169}$GADAEKPFpYVNVEFHHE$_{185}$ for pBCR, $_{169}$GADAEKPFYVNVEFHHE$_{185}$ for BCR, $_{1060}$DTFLPVPEpYINQSVPKR$_{1076}$ for pEGFR, and $_{1060}$DTFLPVPEYINQSVPKR$_{1076}$ for EGFR) (Fig. 2 *c*), the length of which can stretch across the interaction surface of the SH2 domains. The pBCR and pEGFR peptides in complex with $SH2^{GRB2}$ were modeled by linearly extending the N- and C-termini of the bound peptides in the crystal structures. Since the original peptides bound to $nSH2^{p85\alpha}$ and $cSH2^{p85\alpha}$ are segments from phosphorylated PDGF receptor (pPDGFR), the sequences of PDGFR residues were converted into that of BCR, and then extended the residues at both ends. The coordinates of unphosphorylated peptides were obtained by removing the phosphate in pY. Mutant peptides were obtained by substituting N179 to Gln (N179Q), Ala (N179A), and Gly (N179G) in the pBCR-$SH2^{GRB2}$ and BCR-$SH2^{GRB2}$ complexes (Fig. 7 *a*). In the modeling, we set positional restraints on the regions of the peptides in the crystal structure (hereafter referred to as middle region) and relaxed the extended regions. Four relaxation cycles were performed on these complexes: 1) 500-step steepest descent minimizations by constraining the middle region with harmonic force constant of 5 kcal/mol/Å^2; 2) 200 steps of steepest descent minimizations by constraining the backbones of the whole complexes (the peptide and the SH2 domain) with harmonic force constant of 5 kcal/mol/Å^2; 3) 200 steps of conjugate gradient minimizations by constraining the backbones of the whole complexes with harmonic force constant of 2 kcal/mol/Å^2; and 4) 200-step minimizations using adopted basis Newton-Raphson without constraining atoms. A total of eight complexes were constructed and solvated using explicit TIP3P water. Counterions of Na^+ and Cl^- were added into the solvated systems to neutralize the systems and mimic 150 mM ionic strength. The modeling process was performed in the CHARMM program (48).

MD simulation protocols

Our simulations were carried out according to the protocol published in our previous works (49–52). Before MD simulations for production, 5000-step

TABLE 1 Details of the eight pY/Y-peptide-SH2 complex systems

PDB:	SH2 domain	Peptide in crystal structure	pY-peptide-SH2	Y-peptide-SH2
1TZE	GRB2	pBCR	pBCR-$SH2^{GRB2}$	BCR-$SH2^{GRB2}$
1ZFP	GRB2	pEGFR	pEGFR-$SH2^{GRB2}$	EGFR-$SH2^{GRB2}$
2IUI	nSH2 of p85α	pPDGFR	pBCR-$nSH2^{p85\alpha}$	BCR-$nSH2^{p85\alpha}$
1H9O	cSH2 of p85α	pPDGFR	pBCR-$cSH2^{p85\alpha}$	BCR-$cSH2^{p85\alpha}$

energetical minimizations were performed to the initial complex systems using the conjugate gradient minimization method to eliminate bad contacts between atoms in the systems. Then, a total of 1 μs all-atom explicit-solvent MD simulations for each system were conducted using NAMD 2.13 package (53) with CHARMM (48) all-atom force field (version 36m) (54,55). The canonical phosphorylation of tyrosine generates negative charge of –2e. The standard CHARMM program provides the topology and parameter for the posttranslational modification on the side chain of the phosphotyrosine. During the MD simulations, NPT ensemble (constant number of atoms, pressure, and temperature) under 3D periodic conditions were applied to each system. The temperature and pressure were kept at 310 K and 1 atm using the Langevin thermostat method with a damping coefficient of 1 ps^{-1} and the Langevin piston control algorithm, respectively. All covalent bonds, including hydrogen atoms, were constrained using the RATTLE method so that the velocity Verlet algorithm was applied to integrate the Newton motion equation with a larger time step of 2 fs. The interaction potentials between atoms were estimated by long-range electrostatic interactions using particle mesh Ewald method with a grading space of 1.0 Å and short-range van der Waals (vdW) interactions using switching functions with the twin-range cutoff at 12 and 14 Å. All MD trajectories were saved each 2 ps for further data analysis. The analysis of the MD simulation results was performed in the CHARMM (48) and VMD packages using the FORTRAN and TCL scripts. To obtain the electrostatic surface of the SH2 domains, we used the adaptive Poisson-Boltzmann solver tool in PyMol (56). To check reproducibility, three replicated simulations were performed for pBCR-$SH2^{GRB2}$, pEGFR-$SH2^{GRB2}$, pBCR-$nSH2^{p85\alpha}$, and pBCR-$cSH2^{p85\alpha}$. The three parallel simulations obtained comparable results. The statistics were collected by averaging over the three replicas. Averages were also taken over the last half of the simulation trajectories. The occupancies of the clustering structures were calculated using UCSF Chimera software (57).

Binding free energy calculations

The binding free energies of the pY-/Y-peptides interactions with the SH2 domains were calculated by molecular mechanics energies combined with the generalized Born surface area continuum solvation method using the CHARMM program (48). In the calculation, we followed our earlier protocol (58–64). The average binding free energy $\langle \Delta G_b \rangle$ for the complex system is a sum of the gas-phase contribution from the molecular mechanics energy $\langle \Delta E_{MM} \rangle$, the solvation energy contribution $\langle \Delta G_{sol} \rangle$, and the entropy contribution $T\Delta S$,

$$\langle \Delta G_b \rangle = \langle \Delta E_{MM} \rangle + \langle \Delta G_{sol} \rangle - T\Delta S,$$

where the angle brackets indicate the average along the last half of the simulations. The gas-phase contribution is a sum of the internal energy ΔH_{inter}, the electrostatic interaction ΔH_{elec}, and the vdW interaction ΔH_{vdW},

$$\Delta E_{MM} = \Delta H_{inter} + \Delta H_{elec} + \Delta H_{vdW}.$$

The solvation free energy ΔG_{sol} contains the nonpolar and electrostatic components, calculated by the GB using the GBSW module (65),

$$\Delta G_{sol} = \Delta G_{sol}^{elec} + \Delta G_{sol}^{nonpolar}.$$

The entropic term can be decomposed into three components, which are the translational contribution $T\Delta S_{trans}$, rotational contribution $T\Delta S_{rot}$, and vibrational contribution $T\Delta S_{vib}$,

$$T\Delta S = T\Delta S_{trans} + T\Delta S_{rot} + T\Delta S_{vib}.$$

The translational and rotational components were estimated from the principal moment of inertia, and the vibrational entropy is calculated based on the quasiharmonic mode in the VIBRAN module of the CHARMM program (48). The change in the binding free energy due to the binding was calculated using the equation,

$$\Delta G_b = G_b^{complex} - \left(G_b^{peptide} + G_b^{SH2}\right).$$

RESULTS

Characterization of pY-/Y-peptides and SH2 domains

It is known that SH2 domains associate with pY of tyrosine kinases to signal downstream to mediate cellular processes. Although the structures of SH2 domains are conserved, they have different binding mode preferences to pY-containing peptides (47,66). In some cases, SH2 domain binding appears independent of tyrosine phosphorylation and is driven by other interactions (67–69). Considering that binding mode and affinity between peptides and SH2 domains highly depend on the interaction interface, we first characterized the surfaces of $SH2^{GRB2}$, the N-terminal SH2 domain of p85α ($nSH2^{p85\alpha}$), and the C-terminal SH2 domain of p85α ($cSH2^{p85\alpha}$) exposed to the peptides. p85α is the regulatory subunit of PI3Kα. $SH2^{GRB2}$, $nSH2^{p85\alpha}$, and $cSH2^{p85\alpha}$ present a similar secondary structure topology with an antiparallel β-sheet formed by βB-, βC-, and βD-strands in the core flanked by two α-helices, αA and αB (Figs. 1 *d* and 2 *a*). They expose two main pockets for phosphopeptide recognition (70), the pY-binding and the specificity pockets. The pY-binding pocket is a conserved hydrophilic pocket to capture the phosphate side chain, which is surrounded by R67, R86, S88, S90, S96, H107, and K109 in $SH2^{GRB2}$, R340, R358, S361, T362, K382, and L380 in $nSH2^{p85\alpha}$, and R631, R639, H669, and V671 in $cSH2^{p85\alpha}$. Two Arg residues at αA and βB, R67 and R86 in $SH2^{GRB2}$, R340 and R358 in $nSH2^{p85\alpha}$, and R631 and R639 in $cSH2^{p85\alpha}$, contribute large portions of the pY interactions (Fig. 2 *b*). Another basic residue at βD, K109 and K382 for $SH2^{GRB2}$ and $nSH2^{p85\alpha}$, respectively, is adjacent to the pY-binding pocket, which favors an additional electrostatic interaction in this pocket. Note that the basic residue is replaced with the hydrophobic residue Val in βD, in $cSH2^{p85\alpha}$. The specificity pocket is capable of accommodating residues located at the C-terminal of pY in peptides, accounting for the binding specificity. The pocket is formed by F108, K109, L120, and W121 in $SH2^{GRB2}$, I381, F392, Y416, and N417 in $nSH2^{p85\alpha}$, and C670, F681, H706, and L710 in $cSH2^{p85\alpha}$ (Fig. 2 *a*). Evidence supports the $SH2^{GRB2}$ specificity pocket preference for Asn (34,69,71). In contrast, both $nSH2^{p85\alpha}$ and $cSH2^{p85\alpha}$ are favorable to Met (72). Some positively charged residues away from the pY-binding pocket of $nSH2^{p85\alpha}$ and $cSH2^{p85\alpha}$ expose large positive surfaces. For $nSH2^{p85\alpha}$, these residues include R348 at αA, R373 and K374 at βC, K379 at βD, K419 in BG loop, and K423 at βG. For $cSH2^{p85\alpha}$, they are R639 at αA, K653 in the BC loop, and K668 at βD (Fig. 2 *b*). The negatively

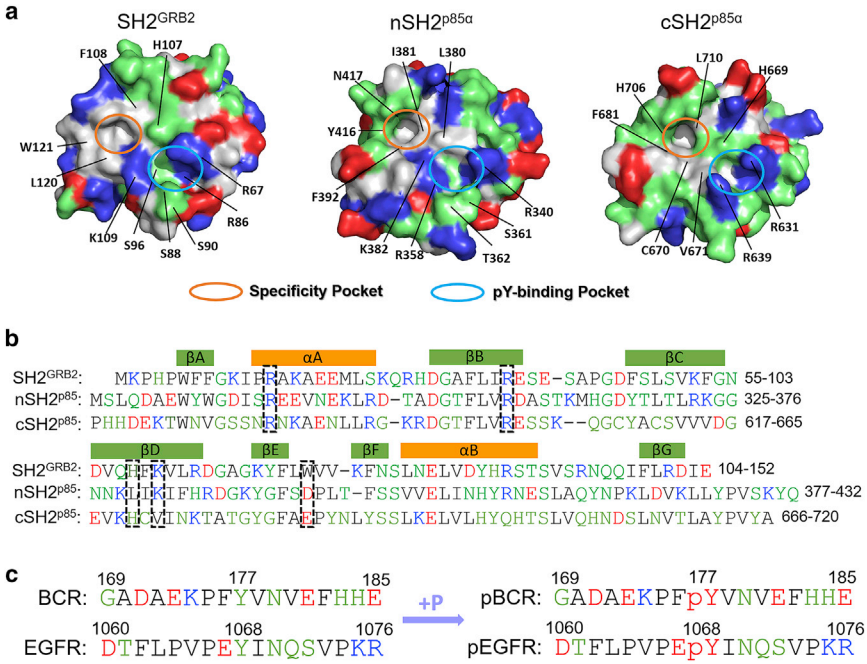

FIGURE 2 Structures and sequences. (*a*) Structures and (*b*) sequences of the $SH2^{GRB2}$, $nSH2^{p85\alpha}$, and $cSH2^{p85\alpha}$ domains. (*c*) Sequences of pBCR, BCR, pEGFR, and EGFR peptides. The positively charged, negatively charged, polar, and hydrophobic residues are colored in blue, red, green, and white/black (structure/sequence), respectively.

charged residues, D665 at βC and E667 at βD, can compensate for some of the $cSH2^{p85\alpha}$ positively charged surface. Experimental studies revealed that $SH2^{GRB2}$ can bind pBCR and pEGFR (refers to phosphorylated tyrosine at position 1068) peptides, followed by downstream Ras activation (41). Residues Y177 in BCR and Y1068 in EGFR, are the binding sites for $SH2^{GRB2}$ (36,38). The recognition areas can be larger than the binding site interfaces, since residues away from pY can play a role in SH2 domain binding. To uncover contextual peptide information for the binding between SH2 domains and the peptides, the 17-residue peptides from pBCR, BCR, pEGFR, and EGFR were used in this work (Fig. 2 *c*). Sequence analysis indicates that both pBCR and pEGFR have Asn at the +2 position C-terminal to pY, which we interpret to be relevant to the specific binding to the $SH2^{GRB2}$ domain.

Binding modes between pY-/Y-peptides and SH2 domains

We constructed models of eight complexes with the four different peptides (pBCR, BCR, pEGFR, and EGFR) and three different SH2 domains ($SH2^{GRB2}$, $nSH2^{p85\alpha}$, and $cSH2^{p85\alpha}$). For each combination of the peptides with the SH2 domains, four complexes were obtained with $SH2^{GRB2}$ (pBCR-$SH2^{GRB2}$, BCR-$SH2^{GRB2}$, pEGFR-$SH2^{GRB2}$, and EGFR-$SH2^{GRB2}$), and two complexes each for $nSH2^{p85\alpha}$ (pBCR-$nSH2^{p85\alpha}$ and BCR-$nSH2^{p85\alpha}$) and for $cSH2^{p85\alpha}$ (pBCR-$cSH2^{p85\alpha}$ and BCR-$cSH2^{p85\alpha}$). Here, we omitted the well-defined interaction between EGFR and p85α, since our focus is on the interactions involving BCR-ABL and/or GRB2. The root mean-square deviation profiles show that the six binding systems (pBCR-$SH2^{GRB2}$ and BCR-$SH2^{GRB2}$, pEGFR-$SH2^{GRB2}$ and EGFR-$SH2^{GRB2}$, and pBCR-$nSH2^{p85\alpha}$ and BCR-$nSH2^{p85\alpha}$) reached equilibration after the initial 100 ns (Fig. S2). During the simulations, we observed that most SH2 domains were stable, keeping the peptides intact, except $cSH2^{p85\alpha}$. Unfavorable binding was observed for pBCR-$cSH2^{p85\alpha}$ (Video S1) and BCR-$cSH2^{p85\alpha}$, which dissociated (Video S2). In contrast, the pBCR and BCR peptides can interact with $nSH2^{p85\alpha}$, displaying a linear peptide topology (Fig. S3). However, the topology of the peptides interacting with $SH2^{GRB2}$ is different from the pBCR and BCR peptides binding to $nSH2^{p85\alpha}$. pBCR, BCR, pEGFR, and EGFR peptides bind to $SH2^{GRB2}$ through the binding motifs in their middle regions, displaying a unique type I β-turn conformation (Figs. 3 and S4), which is in line with the peptide conformations in the crystal structures (Fig. S1) (36,38). The specific binding of the peptides indicates that the $SH2^{GRB2}$ specificity pocket accommodates Asn at the +2 position C-terminal to pY/Y, inducing the kinked peptide structure. However, the specificity the pocket is absent in $nSH2^{p85\alpha}$, suggesting that the peptides' interactions with $nSH2^{p85\alpha}$ are independent of the specific binding. Presumably, this binding can be attributed to electrostatic interaction between the negatively charged residues in pBCR/BCR and the exposed, positively charged residues in $nSH2^{p85\alpha}$, and the cross-reactivity of the pYVNV motif toward the nSH2 domain (34). To characterize the dynamics for the eight systems, we calculated the distances between N179/N1070 and the specificity pocket (D1), and between pY177/Y177/pY1068/Y1068 and the pY-binding pocket (D2). D1 is short and stable for pBCR-$SH2^{GRB2}$ (4.8 ± 0.3 Å), BCR-$SH2^{GRB2}$ (4.8 ± 0.3 Å), pEGFR-$SH2^{GRB2}$

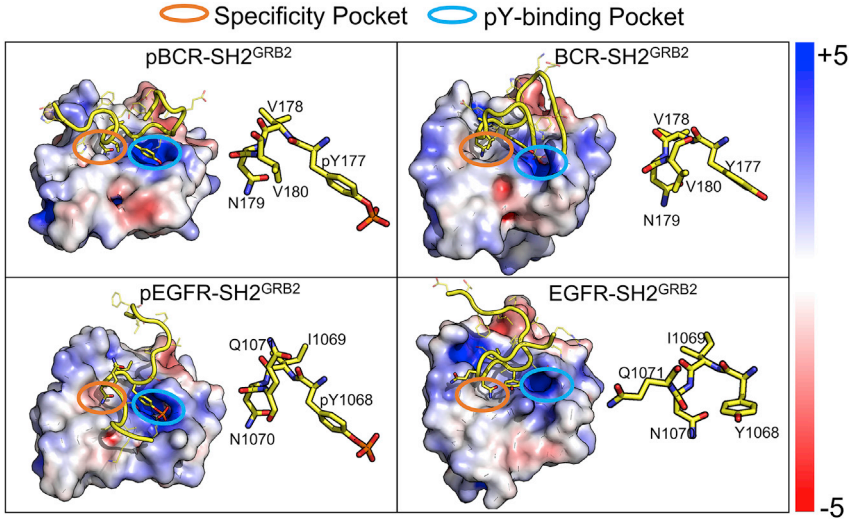

FIGURE 3 Unique binding modes between pY/Y-peptides and $SH2^{GRB2}$. In the cartoons, $SH2^{GRB2}$ is shown in electrostatic surface, and the peptides in the bound state are represented as yellow tubes on $SH2^{GRB2}$. The color bar denotes the charge properties (*red*, *negative charge*; *blue*, *positive charge*), characterizing the electrostatic surfaces of the $SH2^{GRB2}$ domain. Stick representations next to $SH2^{GRB2}$ denote the peptide structures with the residues involved in the β-turn region. Four β-turn residues are marked on each peptide. The cartoon structures of the protein represent the averaged structures over the last half of the simulations. The representative structures account for 72.4, 66.8, 61.6, and 68.0% of the ensemble structures over the last half of the trajectories for pBCR-$SH2^{GRB2}$, BCR-$SH2^{GRB2}$, pEGFR-$SH2^{GRB2}$, and EGFR-$SH2^{GRB2}$, respectively.

(4.9 ± 0.5 Å), and EGFR-$SH2^{GRB2}$ (5.0 ± 0.4 Å), in contrast to the longer D1 for pBCR-$nSH2^{p85\alpha}$ (6.4 ± 0.3 Å) and BCR-$nSH2^{p85\alpha}$ (6.1 ± 0.6 Å) (Fig. S5). This indicates that N179 in pBCR and BCR, and N1086 in pEGFR and EGFR, keep their positions intact favoring the interaction in the specificity pocket of $SH2^{GRB2}$ (Fig. 3), while N179 in pBCR and BCR shifts away from the specificity pocket of $nSH2^{p85\alpha}$ (Fig. S3). D2 does not present significant change for pBCR-$SH2^{GRB2}$ (8.5 ± 0.6 Å), BCR-$SH2^{GRB2}$ (9.5 ± 0.6 Å), pEGFR-$SH2^{GRB2}$ (8.9 ± 0.4 Å), EGFR-$SH2^{GRB2}$ (9.0 ± 0.6 Å), and pBCR-$nSH2^{p85\alpha}$ (8.6 ± 0.3 Å) due to no displacement occurring to pY/Y in pBCR/BCR and pEGFR/EGFR for these cases. However, D2 shows larger fluctuations for BCR-$nSH2^{p85\alpha}$ (10.9 ± 1.1 Å), since Y177 in BCR loses its interaction with the pY-binding pocket of $nSH2^{p85\alpha}$. Although no immediate dissociation was observed for pBCR from $cSH2^{p85\alpha}$, unfavorable binding is evident from the apparent displacement of pY177 and N179 (Fig. S5) and the large fluctuation of pBCR in the interaction with $cSH2^{p85\alpha}$ (Fig. S6). Taken together, the nonspecific binding of $nSH2^{p85\alpha}$ and unstable association of $cSH2^{p85\alpha}$ suggest that the interaction of p85α of PI3Kα with BCR-ABL is less likely to be populated. EGFR providing multiple pY-binding motifs can easily compete with BCR-ABL, recruiting PI3Kα to the membrane. Thus, our attention is mainly focused on the interactions of GRB2 with BCR-ABL and EGFR.

To determine whether these peptides can maintain a stable type I β-turn conformation (Fig. S7 *a*) when bound to the $SH2^{GRB2}$ domain, we calculated the distance ($D_{C\alpha(i)\text{-}C\alpha(i+3)}$) between Cα in residue i (pY/Y) and Cα in residue i+3 (pY/Y +3) (Fig. S7 *b*), and the torsion angles φ and ψ for residue i+1 (φ_1 and ψ_1) and residue i+2 (φ_2 and ψ_2) (Fig. S7 *c*). Type I β-turn conformation, defined by $D_{C\alpha(i)\text{-}C\alpha(i+3)}$, is less than 7 Å and the torsion angles φ_1, ψ_1, φ_2, and ψ_2 are ∼−60, ∼−30, ∼−90, and ∼0°, respectively (73). In our simulations, $D_{C\alpha(i)\text{-}C\alpha(i+3)}$ and $\varphi_1/\psi_1/\varphi_2/\psi_2$ are 5.83 Å and −67.2°/−33.0°/−90.5°/−6.4° for pBCR, 5.75 Å and −67.9°/−39.5°/−95.9°/−1.69° for BCR, and 5.81 Å and −67.0°/−42.0°/−92.3°/4.6° for pEGFR, satisfying all criteria of type I β-turn conformation. However, although torsion angles $\varphi_1/\psi_1/\varphi_2$ (−70.7°/−41.5°/−86.5°) for EGFR in complex with $SH2^{GRB2}$ can roughly meet the criteria of type I β-turn conformation, $D_{C\alpha(i)\text{-}C\alpha(i+3)}$ = 7.22 Å is greater than 7 Å, and ψ_2 = 135.1° largely deviates from 0°. This indicates an unstable type I β-turn conformation of EGFR when bound to the SH2 domain of GRB2.

pY motifs in GRB2 SH2 domain binding

In vivo, $SH2^{GRB2}$ can specifically recognize the pY motifs of many proteins. These motifs share sequence similarities. However, recognition of a pY motif by one SH2 domain over another is determined by residues at the positions +1 to +5 C-terminus to pY (71). The pYXN motif is usually regarded as $SH2^{GRB2}$-binding motif (34,69,71). For a protein binding to GRB2, the binding motif dominates the interaction. To identify motif residues contributing to the interaction, we calculated the contact probability between the peptide residues and the $SH2^{GRB2}$ residues (Fig. 4 *a*). A contact event is determined if the minimum distance between a peptide residue and a $SH2^{GRB2}$ residue is less than 3.5 Å. We identified residues with contact probability ≥60%: F176, pY177, V178, N179, V180, F182, and E185 in pBCR, F176, Y177, V178, N179, V180, and E185 in BCR, E1067, pY1068, I1069, and N1070 in pEGFR, and E1067, Y1068, I1069, and N1070 in EGFR (Table S1). Based on the calculations, we obtained the five-residue motifs of $_{176}$FpYVNV$_{180}$ for pBCR and $_{176}$FYVNV$_{180}$ for BCR, and four-residue motifs of $_{1068}$EpYIN$_{1071}$ for pEGFR and $_{1068}$EYIN$_{1071}$ for EGFR in the interaction with $SH2^{GRB2}$ (Fig. 4 *b*).

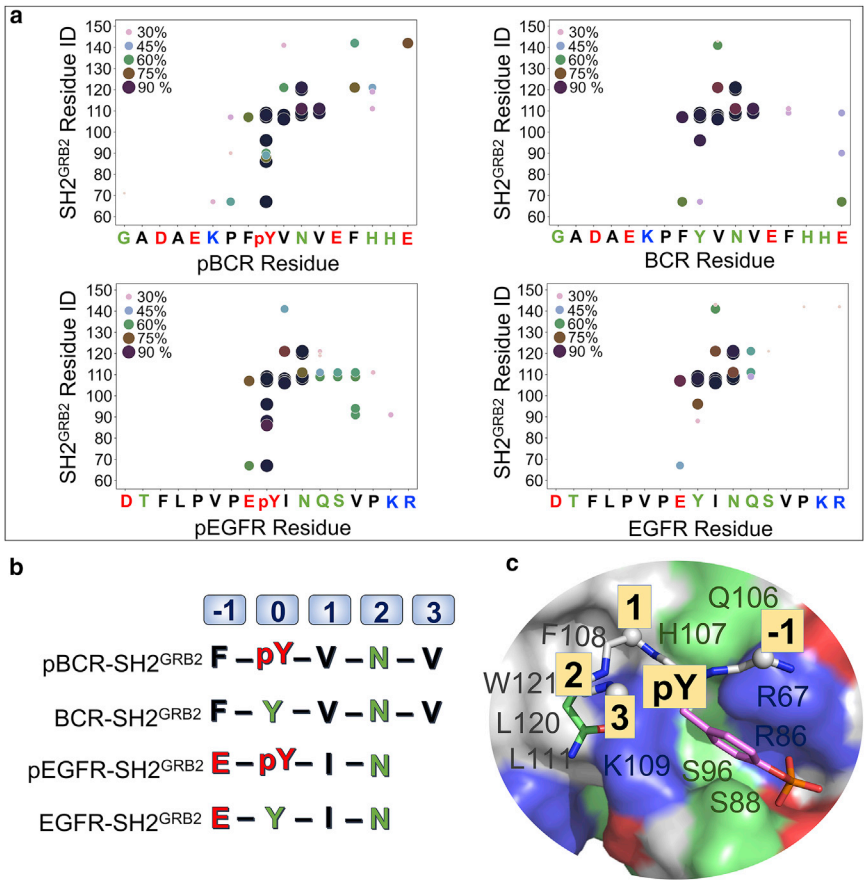

FIGURE 4 $SH2^{GRB2}$-binding motifs of pY/Y-peptides. (*a*) Intermolecular contact probability (%) of paired residues for pBCR-$SH2^{GRB2}$, BCR-$SH2^{GRB2}$, pEGFR-$SH2^{GRB2}$, and EGFR-$SH2^{GRB2}$ systems. A contact event is determined if the minimum distance between a peptide residue and a $SH2^{GRB2}$ residue is less than 3.5 Å, otherwise a separation event. This calculation includes the hydrogen atoms. The contact events were counted every 10 ps, and the contact probability is calculated by the summation of contact events divided by all events (contact and separation) during the simulations. (*b*) $SH2^{GRB2}$-binding motifs of pBCR, BCR, pEGFR, and EGFR. (*c*) Cartoon representing the precise residue-residue interactions between the motifs of pY-peptide and $SH2^{GRB2}$.

In signal transduction, proteins often utilize the GRB2 adaptor protein to link extracellular signal to downward signaling pathways through the interaction between the pYXN motif and $SH2^{GRB2}$. To further understand the pY motif interaction with $SH2^{GRB2}$ in terms of specificity and affinity, we collected the pY motifs in different proteins with experimentally measured affinities to $SH2^{GRB2}$ from the literature (Table S2). All motifs have the conserved Asn at the +2 position C-terminal to pY. Residues at the +1 and +3 positions are diverse, suggesting that residues at the +1 and +3 positions have smaller impacts on the specificity compared with the residue at the +2 position. Kessels et al. used a solid-phase peptide library for the selection of the $SH2^{GRB2}$-binding motifs based on affinity and specificity (Fig. S8 *a*) (34). Their results confirmed the strong selection for Asn at the +2 position for $SH2^{GRB2}$-specific recognition, but a weaker bias at the +1 and +3 positions (34). They identified Gln, Glu, and Val at the +1 position as the most favorable for binding affinity. Peptide ligands containing basic residues Lys and Arg at this position exclusively interact with $SH2^{GRB2}$ and lose the cross-reactivity toward other SH2 domains. $SH2^{GRB2}$-binding motifs with the hydrophobic residues at the +3 position show higher affinity to $SH2^{GRB2}$ (34,74), due to the favorable interaction with L111 in $SH2^{GRB2}$ as observed in our simulations (Table S1). The four hydrophobic residues, Ile, Leu, Val, and Phe at the +3 position, yield the most favorable affinity between the ligands and $SH2^{GRB2}$ with the contribution to affinity in the order of Leu > Ile > Val > Phe. Based on these results, they recognized the binding motifs of pY-Q/E-N-L/I with optimal affinity and pY-K/R-N-I/L with optimal specificity for the binding of $SH2^{GRB2}$. However, the pYVNV motif was consistently observed with high affinity to $SH2^{GRB2}$ in different library selections, even outperforming the proposed pYQNL motif (34). The pYVNV motif can be found in BCR, SHC, and LAT, etc. (Table S2). These proteins are involved in cell signaling and known to interact with GRB2. The pYENV motif with Glu at the +1 position induces stronger mean fluorescence intensity than pYVNV with Val at the +1 position (34). This confirms that the negatively charged residues at the +1 position favor a higher affinity than the hydrophobic residue of Val, probably through hydrogen bond (H-bond) formation and electrostatic interaction with K109 in $SH2^{GRB2}$ (75). Such an interaction likely assists that occurring in the pY-binding pocket. On the other hand, the hydrophobic residues at the +1 position can form a hydrophobic core with F108 in $SH2^{GRB2}$, favoring the interaction in the specificity pocket. We speculate that the negatively charged Glu at the +1 position is most conducive to the binding affinity, followed by Val. The pYVNI motif

with Ile at the +3 position generates stronger affinity for binding $SH2^{GRB2}$ than the pYVNV motif with Val at this position (Fig. S8 *a*). The hydrophilic residue at this position as in the pYINQ motif of EGFR is not favorable for the interaction (Fig. 3). This verified that pEGFR has lower binding affinity to $SH2^{GRB2}$ than pBCR with the pYVNV motif (34,38). In addition to residues at the +1 and +3 positions C-terminal to pY, we observed that the residue at the −1 position N-terminal to pY plays a significant role in binding $SH2^{GRB2}$. The residue at the −1 position N-terminal to pY is between residues R67 and H107 in $SH2^{GRB2}$ (Fig. 4 *c*). The hydrophobic residue F176 at the −1 position in pBCR intermittently forms intermolecular π-π stacking with H107 or F108 in $SH2^{GRB2}$, while the phosphate in pY is secured by three basic residues R67, R86, and K109 in the pY-binding pocket of $SH2^{GRB2}$ through salt bridge interactions (Fig. S9). The corresponding residue at the −1 position in pEGFR is E1067. The negatively charged residue removes R67 from the pY-binding pocket and forms a salt bridge with it, resulting in the pY phosphate being surrounded by two basic residues R86 and K109 in the $SH2^{GRB2}$ pocket. However, with an added salt bridge formation by E1067 near the pY-binding pocket, the overall electrostatic interaction scheme is conserved. Taken together, we propose that candidates for the −1 position N-terminal to pY can be negatively charged residues. Positively charged residues at this position may not be candidates, since electrostatic repulsion by R67 in $SH2^{GRB2}$ may occur, interfering with the interaction in the pY-binding pocket. Our proposed five-residue motif with optimal binding affinity to $SH2^{GRB2}$ is E/D-pY-E/V-N-I/L (Fig. S9 *b*). However, selection for the residue at the −1 position requires further verification by experiments or computations.

Interactions between pY/Y-peptides and the GRB2 SH2 domain

To quantify the binding affinities between the peptides and $SH2^{GRB2}$, we employed molecular mechanics energies combined with the generalized Born surface area continuum solvation (Fig. 5 *a*). The average binding free energy, $\langle \Delta G_b \rangle$, is the summation of three components, the solvation energy $\langle \Delta G_{sol} \rangle$, the gas-phase molecular mechanics energy $\langle \Delta E_{MM} \rangle$, and the conformational entropy $-T\Delta S$ contributions, where the angle brackets denote the average along the simulation trajectories. The calculated binding free energies due to the formation of the complex are ∼−30.2 and ∼−22.3 kcal/mol for pBCR-$SH2^{GRB2}$ and pEGFR-$SH2^{GRB2}$, respectively, which are much lower than their unphosphorylated counterparts, ∼−1.1 and ∼0.5 kcal/mol for BCR-$SH2^{GRB2}$ and EGFR-$SH2^{GRB2}$, respectively. The unfavorable solvation energies (∼714.1 kcal/mol for pBCR-$SH2^{GRB2}$, ∼326.6 kcal/mol for BCR-$SH2^{GRB2}$, ∼421.0 kcal/mol for pEGFR-$SH2^{GRB2}$, and ∼80.7 kcal/mol for EGFR-$SH2^{GRB2}$) and the favorable molecular mechanics energies in gas phase (∼−791.0 kcal/mol for pBCR-$SH2^{GRB2}$, ∼−374.3 kcal for BCR-$SH2^{GRB2}$, ∼−491.0 kcal/mol for pEGFR-$SH2^{GRB2}$, and ∼−126.0 kcal/mol for EGFR-$SH2^{GRB2}$) mostly contribute to the binding free energy for the four systems. The conformational entropy ($-T\Delta S$) has a negligible impact on the discrepancy of the binding free energy, as demonstrated by the subtle difference of the conformational entropy ranging from ∼45.8 to ∼47.7 kcal/mol. This might result from a similar binding mode for the four systems (Fig. 3). Furthermore, we calculated the interaction energies without consideration of the conformational entropy and the solvation effect, between the four peptides and $SH2^{GRB2}$ (Fig. 5 *b*). They show a similar trend with the binding free energies, exhibiting much lower interaction energies for the phosphorylated peptide-binding systems (∼−618.4 kcal/mol for pBCR-$SH2^{GRB2}$ and ∼−433.4 kcal/mol for pEGFR-$SH2^{GRB2}$) than that for the unphosphorylated peptide-binding systems (∼−220.7 kcal/mol for BCR-$SH2^{GRB2}$ and ∼−142.5 kcal/mol for EGFR-$SH2^{GRB2}$). This scenario further confirms the minor effect of conformational changes of the peptides on the binding affinity difference among the four different systems. Both the binding free energies and the interaction energies demonstrate that pBCR-$SH2^{GRB2}$ has stronger affinity than pEGFR-$SH2^{GRB2}$, in agreement with experimental data (34,38). Results from the ELISA competition binding assay showed that the pBCR sequence can inhibit the binding between $SH2^{GRB2}$ and pEGFR (38), indicating that pBCR has stronger affinity to $SH2^{GRB2}$ than pEGFR. For the four binding cases, the electrostatic interaction is a major contributor to the total interaction energy, which accounts for 95.0, 86.1, 90.8, and 74.9% for pBCR, BCR, pEGFR, and EGFR interacting with $SH2^{GRB2}$, respectively (Fig. 5 *c*). The vdW interactions show relatively minor contribution to the total interaction energy (5.0, 13.9, 9.2, and 25.1% for pBCR, BCR, pEGFR, and EGFR interacting with $SH2^{GRB2}$, respectively). In the absence of pY, the BCR and EGFR peptides reduced the electrostatic interaction with $SH2^{GRB2}$, compared with the corresponding pY-binding systems.

To identify key residues in $SH2^{GRB2}$ which are responsible for the binding, we calculated intermolecular residue pair interaction energies for the four complexes (Table S3). Some residue pairs showed favorable interactions, particularly for pY177 in pBCR and pY1068 in pEGFR, with high preference for the three basic residues (R67, R86, and K109) in the pY-binding pocket (Fig. 6 *a*). Relatively weak residue pair interactions were observed for the two unphosphorylated peptide-binding systems. Apart from the nonbonded interactions, H-bond formation is also essential for stabilizing the peptides on the $SH2^{GRB2}$ surface. Furthermore, we identified H-bonds between the peptide and $SH2^{GRB2}$ residues with occupancy greater than 50% during the simulations (Table S4). Three locations of stable H-bonds between the binding motifs and $SH2^{GRB2}$ were found for the phosphorylated peptide-binding systems, while two locations of stable H-bonds were identified for the unphosphorylated peptide-binding systems (Fig. 6 *b*). The first location for H-bond formation is common

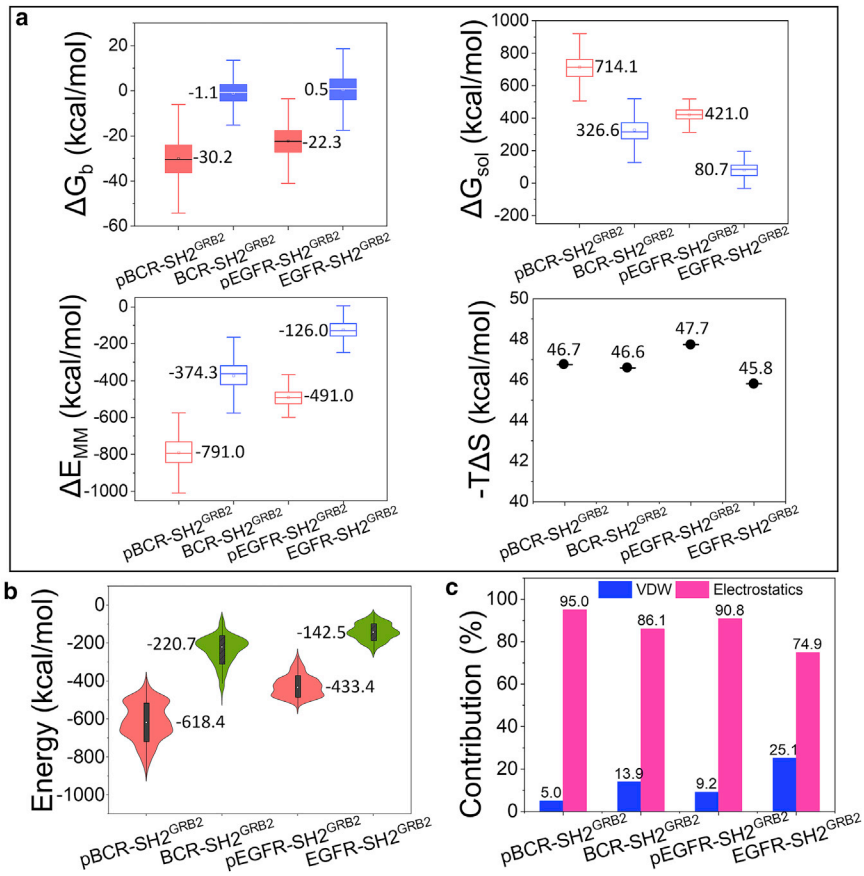

FIGURE 5 Interactions between pY/Y-peptides and $SH2^{GRB2}$. (*a*) Binding free energy, $\langle \Delta G_b \rangle$, combining the contributions of the solvation energy, $\langle \Delta G_{sol} \rangle$, the gas-phase molecular mechanics energy, $\langle \Delta E_{MM} \rangle$, and the conformational entropy, $-T\Delta S$. (*b*) Interaction energies and (*c*) contribution percentage (%) of the decomposed components of vdW and electrostatic energies for pBCR-$SH2^{GRB2}$, BCR-$SH2^{GRB2}$, pEGFR-$SH2^{GRB2}$, and EGFR-$SH2^{GRB2}$ systems. The bars in (*a*) denotes the data range.

for all four complex systems. Regardless of the tyrosine phosphorylation, all four complex systems contain three H-bonds between the side chain of Asn at the +2 position (N179 in pBCR/BCR and N1070 in pEGFR/EGFR) and the backbone residues in the specificity pocket of $SH2^{GRB2}$. These are HD21:Asn*-O:K109, HD22:Asn*-O:L120, and OD1:Asn*-HN:K109, where Asn* denotes the residues in all four peptides. These three H-bonds stabilize the Asn residue in the specificity pocket. The H-bonds at the second location involve backbone atoms between the residue at the +1 position (V178 in pBCR/BCR and I1069 in pEGFR/EGFR) and H107 of $SH2^{GRB2}$, which are HN:V178-O:H107 and HN:I1069-O:H107. The third location for H-bond formation only exists for the phosphorylated peptide-binding systems. A large number of H-bonds were observed in the pY-binding pocket of $SH2^{GRB2}$. The H-bonds occur between the phosphate group of pY in pY-peptide and the $SH2^{GRB2}$ residues, R67, R86, S88, S96, S90, and K109 (Table S4).

Bilateral factors required for the interaction in the specificity pocket

We observed that the BCR and EGFR peptides without pY also can stably bind to $SH2^{GRB2}$ with Asn at the +2 position, morphologically fitting into the specificity pocket, which is independent from tyrosine phosphorylation. This emphasizes the Asn residue at this position for the interaction in the specificity pocket. The importance of this residue for pY-peptide-$SH2^{GRB2}$ specific binding is supported by affinity assay with mutated Asn to Gln (N1070Q) in the pEGFR peptide. Results showed that wild-type pEGFR exhibits reduced binding capability to GRB2 compared with N1070Q pEGFR (38). In a similar vein, we introduced three mutations in the pBCR and BCR peptides by substituting N179 to Gln (N179Q), Ala (N179A), and Gly (N179G) (Fig. 7 *a*). We performed additional simulations for six mutant systems and calculated the binding free energy for the complexes (Fig. 7 *b*). Consistent with the affinity assay results (38), N179Q substitution greatly reduces the binding affinity, as demonstrated by the 66.8% increase in binding free energy for $pBCR_{N179Q}$-$SH2^{GRB2}$ (−10.0 kcal/mol) compared with the wild-type pBCR-$SH2^{GRB2}$ (−30.2 kcal/mol) (Fig. 5 *a*). Visual inspection of the conformational ensembles during the simulation revealed that the C-terminus of $pBCR_{N179Q}$ was quickly repelled by $SH2^{GRB2}$, which is driven by Q179 jumping out of the specificity pocket (Fig. 7 *c*). The interaction in the pY-binding pocket prevented complete dissociation of the peptide from $SH2^{GRB2}$. Although both N179A and N179G substitutions lead to marginal increase in the binding free energy for $pBCR_{N179A}$-$SH2^{GRB2}$ (−29.6 kcal/mol) and

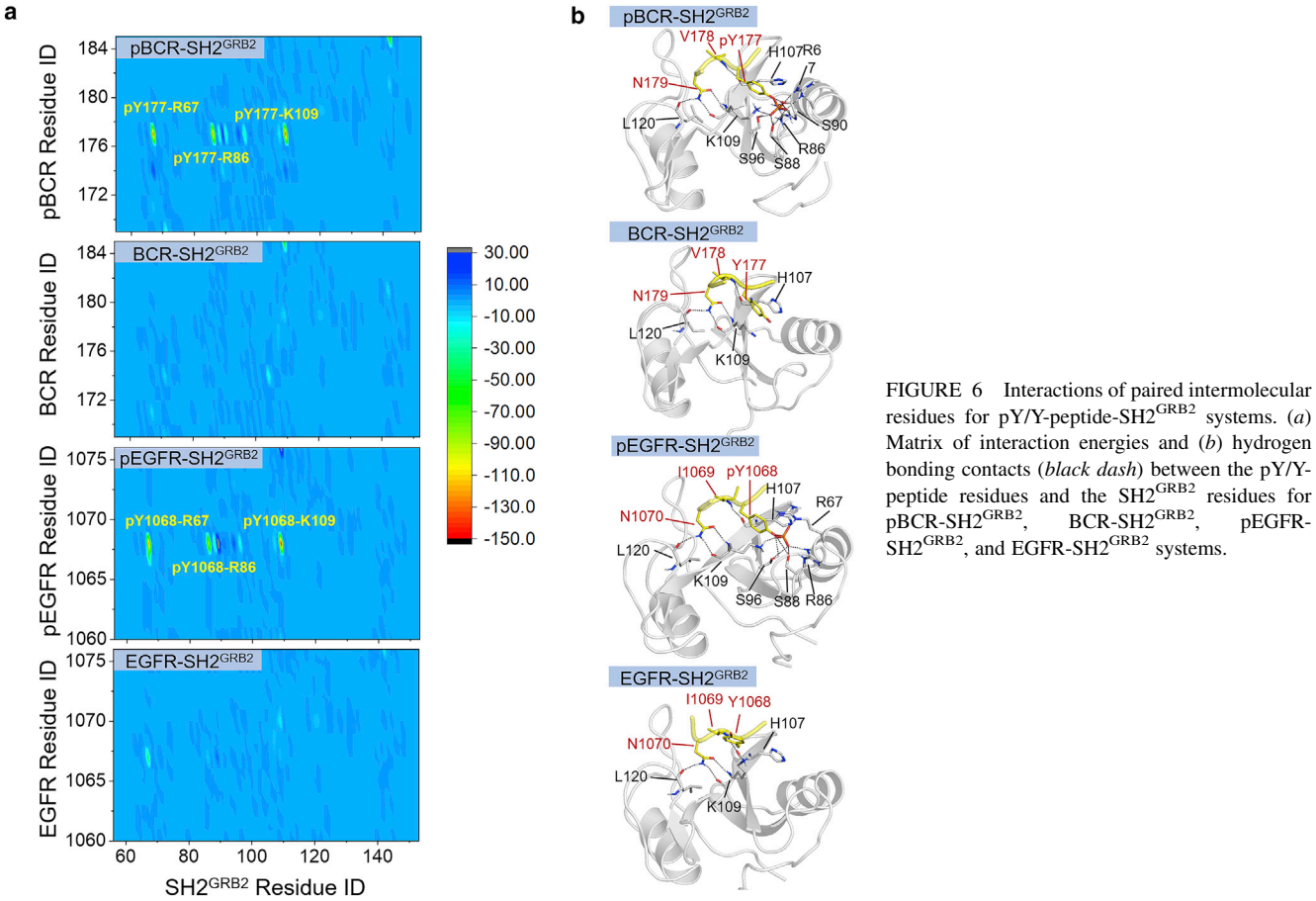

FIGURE 6 Interactions of paired intermolecular residues for pY/Y-peptide-SH2^{GRB2} systems. (*a*) Matrix of interaction energies and (*b*) hydrogen bonding contacts (*black dash*) between the pY/Y-peptide residues and the SH2^{GRB2} residues for pBCR-SH2^{GRB2}, BCR-SH2^{GRB2}, pEGFR-SH2^{GRB2}, and EGFR-SH2^{GRB2} systems.

pBCR$_{N179G}$-SH2^{GRB2} (−22.2 kcal/mol), the phosphorylated mutant peptides were unstable on the surface of SH2^{GRB2}, losing the interaction in the specificity pocket. Similarly, the interaction in the pY-binding pocket prevented dissociation of pBCR$_{N179A}$ and pBCR$_{N179G}$ from SH2^{GRB2}. The mutant peptides without tyrosine phosphorylation, BCR$_{N179Q}$, BCR$_{N179A}$, and BCR$_{N179G}$ almost lost their binding ability to SH2^{GRB2}, yielding drifting and dissociating peptide conformations. These observations confirm the determinant roles of tyrosine phosphorylation in the pY-binding pocket and N179 in the specific binding pocket of SH2^{GRB2}.

We demonstrated that N179 plays an essential role in specific binding of pBCR and SH2^{GRB2}. Characterization of SH2^{GRB2} showed that the specificity pocket is formed by F108, K109, L120, and W121 (Fig. 2 *a*). W121 in the EF loop of SH2^{GRB2} is thought to be a regulator of binding specificity, since its flexibility allows controlling the conformation change of the specificity pocket. Experimental results by isothermal titration calorimetry analysis for wild-type GRB2 and mutant GRB2$_{W121G}$ with their cognate peptides showed that the substitution of W121 by Gly led to lower the binding enthalpy for the SpYVNVQ peptide to GRB2$_{W121G}$ than to wild-type GRB2. To decipher how W121 influences the interaction in the specificity pocket, we characterized the dynamic behavior of W121 in SH2^{GRB2} by calculating the distance, $d_{N\text{-}W121}$, between Cα atom of N179 ($C\alpha^N$) in pBCR/BCR (N1070 in pEGFR/EGFR) and C6 atom of indole group of W121 ($C6^W$) in SH2^{GRB2}. Three relative positions of W121 with respect to the Asn are opposite-down, parallel, side-down positions (Fig. 8 *a*). The parallel position generates the shorter $d_{N\text{-}W121}$, leading to the closed conformation of the specificity pocket. In contrast, the opposite-down and side-down positions produce the longer $d_{N\text{-}W121}$, giving rise to an open conformation of the specificity pocket. The high density of shorter $d_{N\text{-}W121}$ (3.8–4.0 Å) in the distribution profile (Fig. 8 *b*) and the consensus behavior of W121 (Fig. 8 *c*) indicate that the specificity pocket of SH2^{GRB2} preferentially adopts the closed conformation for the binding of pBCR, BCR, pEGFR, and EGFR. In sharp contrast, W121 in SH2^{GRB2} shows stronger perturbation in the binding of pBCR$_{N179Q}$ and pBCR$_{N179A}$ (Fig. S10), leading to conformational alteration of the specificity pocket between the closed and open states.

DISCUSSION

In this work, we present the structural basis for the specific binding of BCR-ABL-GRB2. We further carry out

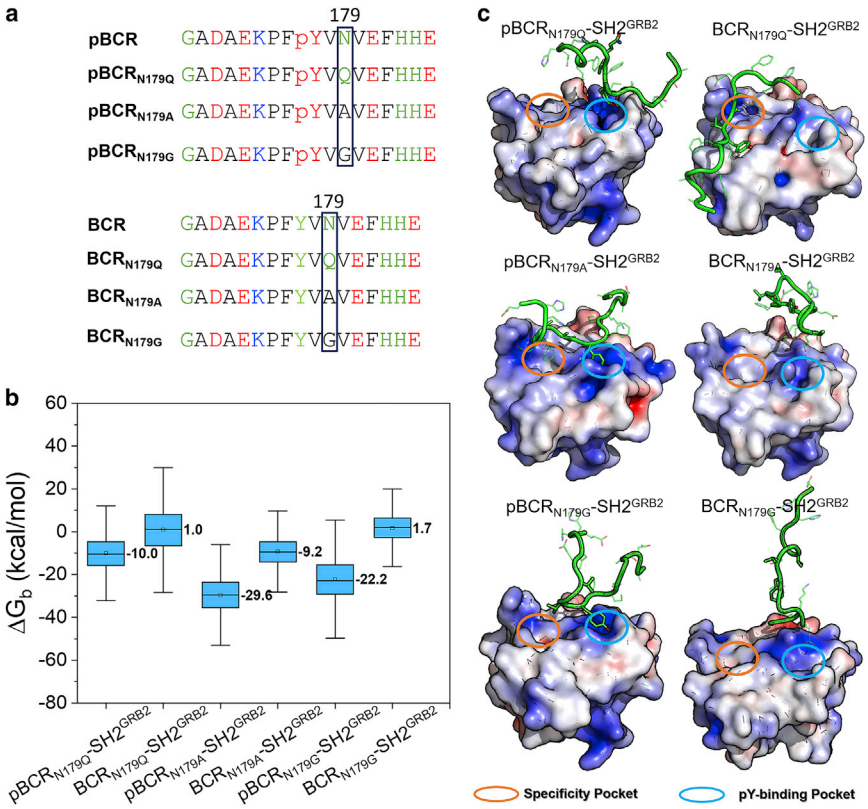

FIGURE 7 Weak or unfavorable binding between mutant pY/Y-peptide and SH2^{GRB2}. (*a*) Sequences of mutant pY/Y-peptides. (*b*) Binding free energies, $\langle \Delta G_b \rangle$, of the mutant pY/Y-peptides interacting with SH2^{GRB2}. (*c*) Representative snapshots for the mutant systems, pBCR$_{N179Q}$-SH2^{GRB2}, BCR$_{N179Q}$-SH2^{GRB2}, pBCR$_{N179A}$-SH2^{GRB2}, BCR$_{N179A}$-SH2^{GRB2}, pBCR$_{N179G}$-SH2^{GRB2}, and BCR$_{N179G}$-SH2^{GRB2}. The cartoon structures of protein represent the snapshots, illustrating the unfavorable interaction. The bars in (*b*) denotes the data range.

computational analysis of the interaction. We compare it with related interactions, where the motif is unphosphorylated and with competitive interaction. We further merge the computational results with available experimental data, to figure out the hallmarks of this specific interaction that drives CML. Our results confirm the experimental data that BCR-ABL can recruit GRB2 through the specific interaction between pBCR containing pY177 and SH2^{GRB2} (21–23,38) and explain exactly how. We extend the data, aiming to make it useful toward predictions, including signaling bypasses in drug resistance and pharmaceutical peptide designs. In CML oncogenesis, BCR and ABL are fused together, releasing ABL's autoinhibition and initiating its kinase activity (Figs. 1 *c* and S11) (76,77). In healthy cells, pEGFR-SH2^{GRB2} specific binding forms the EGFR/GRB2/SOS complex that activates the Ras/MAPK pathway. In CML cells, active BCR-ABL phosphorylates BCR's Y177. BCR's pY177 motif recruits GRB2 through the interaction with the SH2^{GRB2} domain. On plasma membrane signaling platforms, both BCR-ABL and EGFR accommodate the pYXN motif, which is recognized by SH2^{GRB2}. We confirmed that SH2^{GRB2} exhibits higher binding affinity to the BCR-ABL motif than to EGFR. The strong interaction of BCR-ABL with GRB2 leads to recruitment of SOS to the plasma membrane, forming a stable BCR-ABL/GRB2/SOS complex. The increased effective local SOS concentration at the myeloid cell membrane increases the number of active Ras proteins, resulting in more potent oncogenic proliferation of blood cells.

Multiple proteins recognize GRB2 through its SH2 domain. All contain the pYXN motif (Table S2). Docking of pY into the SH2^{GRB2} pocket contributes dominantly to the binding affinity. However, affinity does not account for the entire picture (36). Binding requires specificity, which is furnished by the SH2^{GRB2} specificity pocket. The specificity pocket favors the Asn in the motif. In our simulations, we observed that Asn residues at the +2 position in the pY motifs of both BCR-ABL and EGFR stably dock into the specificity pocket of SH2^{GRB2}. Twofold docking by the pY motif, at the pY-binding pocket and at the specificity pocket, constrained the structure of the protein segment containing the pY motif to type I β-turn conformation. In BCR-ABL, substitutions of Asn to Gln (N179Q), Ala (N179A), and Gly (N179G) abolished the docking of the pY motif into the specificity pocket, consistent with experimental data on the N1070Q mutation in the pY motif of EGFR (38). We map a detailed scenario of the interaction of proteins containing the pY motif with GRB2 (Fig. 9). The high-affinity interaction suggests that, population-wise, pY predominantly initially drives binding with GRB2 through docking into the pY-binding pocket in the SH2 domain, followed by the Asn docking into the specificity pocket. In the pY-binding pocket, pY forms several H-bonds and salt bridges with surrounding residues, offering a major anchor

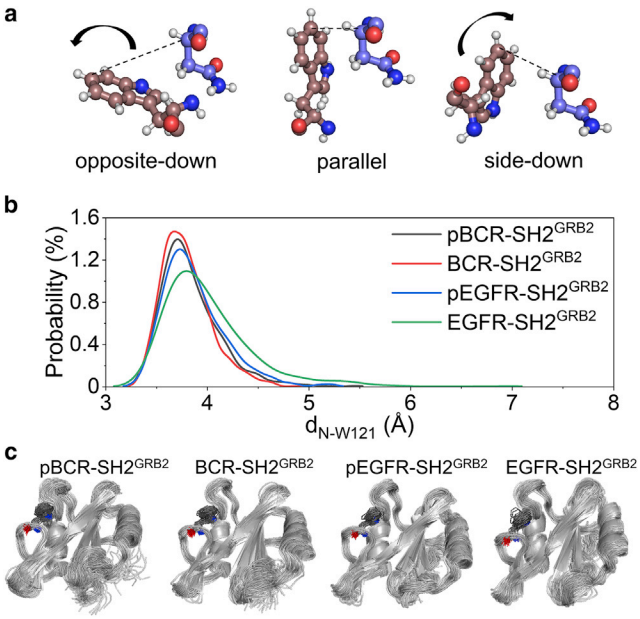

FIGURE 8 Importance of W121 in $SH2^{GRB2}$ for the interaction in the specificity pocket. (*a*) Three different positions/orientations of W121 side chain to Asn at the +2 position C-terminal to pY/Y-peptide. (*b*) Probability distribution functions of the distance between W121 and Asn, $d_{N\text{-}W121}$, and (*c*) superimposed snapshots representing the dynamic behaviors of W121 side chain for pBCR-$SH2^{GRB2}$, BCR-$SH2^{GRB2}$, pEGFR-$SH2^{GRB2}$, and EGFR-$SH2^{GRB2}$. In (*c*), W121 is shown as sticks, in which the blue and red colors denote the oxygen and nitrogen atoms, respectively.

point in $SH2^{GRB2}$. In the specificity pocket, Asn side chain forms three H-bonds with the backbone atoms of K109 and L120. These H-bond formations provoke reorientation of the side chain of W121 in the EF loop of SH2, causing a conformational alteration of the specificity pocket from the open to the closed conformation. This further enhances the interaction of Asn in the specificity pocket, offering another anchor point in $SH2^{GRB2}$. The bulk indole group of W121 can produce steric barrier to hinder the residue at the +3 position, conferring the type I β-turn conformation of the pY motif. Inversely, such conformation helps the specificity pocket to maintain the closed conformation, since no residue after the +2 position can push W121 down to open the pocket. The bilateral interaction in the specificity pocket underscores the paramount role of conformational selection in the specific recognition between the pY motif and $SH2^{GRB2}$.

Both pY motifs of BCR-ABL and EGFR exhibit binding specificity to the SH2 domain, but with different affinities. We identified the five-residue pY motif, FpYVNV, for BCR-ABL, and the four-residue pY motif, EpYIN, for EGFR as responsible for the GRB2 binding. Design efforts centered on pY-peptide-based inhibitors targeting mainly SH2 residues at positions pY +1, +2, and +3, but focused less on the role of the residue at the −1 position (47,71,78,79). Different than earlier works stressing-binding motifs residues C-terminal to pY, our study highlights

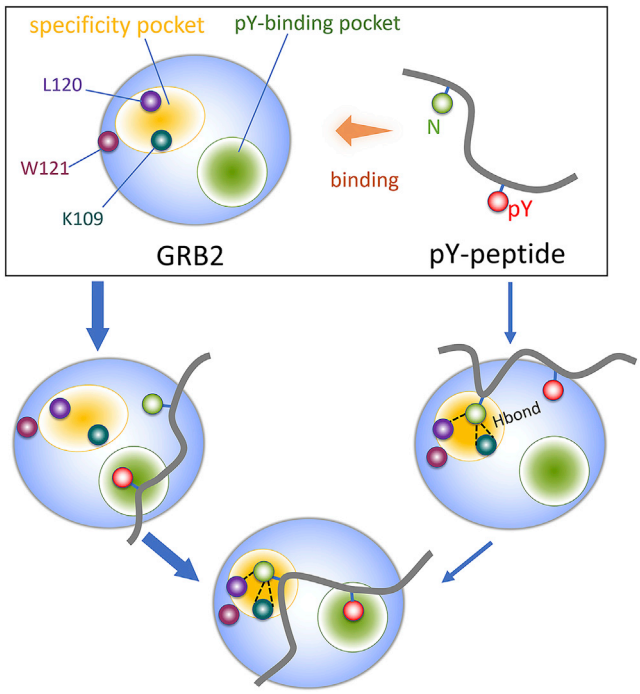

FIGURE 9 Schematic diagram representing the interaction in the specificity pocket of $SH2^{GRB2}$.

the critical role of the residue at the −1 position N-terminal to pY. Since the residue at this position is close to pY, it can positively or negatively influence SH2 binding. It was recognized that a short pY-peptide with five amino acids is sufficient to compete with larger protein-protein interactions (80). Thus, combining our results with earlier experimental data, we propose that E/D-pY-E/V-N-I/L can be a superior $SH2^{GRB2}$ pY-binding motif.

The new insights that our work provide not only help explain experimental results indicating specific binding of pBCR-ABL to GRB2 through its SH2 domain, but also lead to new and experimentally testable hypotheses that the five-residue E/D-pY-E/V-N-I/L motifs can be promising high-affinity inhibitors of $SH2^{GRB2}$ in BCR-ABL-induced signal transduction via the Ras/MAPK pathway, and thus cell proliferation.

CONCLUSIONS

To conclude, we identified the five-residue motif of $_{176}$FpYVNV$_{180}$ as the basis for the specific recognition of the GRB2 SH2 domain at the atomic level. This recognition is essential for the induction of CML through the Ras/MAPK pathway. Phosphorylation of Y177 in BCR triggers binding between BCR-ABL and GRB2 via strong electrostatic interaction in the $SH2^{GRB2}$ pY-binding pocket. N179 in the BCR-ABL pY motif determines whether BCR-ABL can be specifically recognized by $SH2^{GRB2}$. The bilateral factors of N179 in BCR-ABL and W121 in $SH2^{GRB2}$ regulate the interaction in the specificity pocket, and thus binding specificity.

Differences in residues adjacent to the pY and Asn at the +2 position affect the binding affinity of the pY motif-containing protein to $SH2^{GRB2}$, explaining why BCR-ABL has higher binding affinity to $SH2^{GRB2}$ than to EGFR. Our proposed five-residue pY motif appears to have an optimal binding affinity to $SH2^{GRB2}$ and details the conformational change upon binding at the specificity pocket.

Taken together, the implications of this study support the BCR-ABL oncoprotein recruitment of GRB2 in CML and signaling via the Ras/MAPK pathway. Our study further details exactly how GRB2 is recruited, provides blueprints for predicting currently known interaction partners that can take over in resistance and delineates the key attributes for productive inhibitor synthesis.

SUPPORTING MATERIAL

Supporting material can be found online at https://doi.org/10.1016/j.bpj.2022.05.030.

AUTHOR CONTRIBUTIONS

Y.L. performed MD simulations, investigated, analyzed data, and wrote the manuscript. H.J., M.Z., C.-J.T., and R.M. conceptualized the methodology, validated, reviewed, and edited the manuscript. R.N. supervised the project, analyzed, investigated, validated, reviewed, and edited the manuscript.

ACKNOWLEDGMENTS

This project has been funded in whole or in part with federal funds from the National Cancer Institute, National Institutes of Health, under contract HHSN261201500003I. The content of this publication does not necessarily reflect the views or policies of the Department of Health and Human Services, nor does mention of trade names, commercial products, or organizations imply endorsement by the US Government. This research was supported (in part) by the Intramural Research Program of the NIH, National Cancer Institute, CCR. The calculations had been performed using the high-performance computational facilities of the Biowulf PC/Linux cluster at the National Institutes of Health, Bethesda, MD (https://hpc.nih.gov/).

DECLARATION OF INTERESTS

The authors declare no competing interests.

REFERENCES

1. Manley, P. W., L. Barys, and S. W. Cowan-Jacob. 2020. The specificity of asciminib, a potential treatment for chronic myeloid leukemia, as a myristate-pocket binding ABL inhibitor and analysis of its interactions with mutant forms of BCR-ABL1 kinase. *Leuk. Res.* 98:106458. https://doi.org/10.1016/j.leukres.2020.106458.
2. Quach, D., G. Tang, …, S. Q. Yao. 2021. Strategic design of catalytic lysine-targeting reversible covalent BCR-ABL inhibitors*. *Angew Chem. Int. Ed. Engl.* 133:17268–17274. https://doi.org/10.1002/ange.202105383.
3. Lindström, H. J. G., and R. Friedman. 2020. The effects of combination treatments on drug resistance in chronic myeloid leukaemia: an evaluation of the tyrosine kinase inhibitors axitinib and asciminib. *BMC Cancer.* 20:397. https://doi.org/10.1186/s12885-020-06782-9.
4. Alves, R., A. C. Gonçalves, …, A. B. Sarmento Ribeiro. 2021. Resistance to tyrosine kinase inhibitors in chronic myeloid leukemia-from molecular mechanisms to clinical relevance. *Cancers.* 13:4820. https://doi.org/10.3390/cancers13194820.
5. Astl, L., and G. M. Verkhivker. 2019. Atomistic modeling of the ABL kinase regulation by allosteric modulators using structural perturbation analysis and community-based network reconstruction of allosteric communications. *J. Chem. Theor. Comput.* 15:3362–3380. https://doi.org/10.1021/acs.jctc.9b00119.
6. Ren, R. 2005. Mechanisms of BCR-ABL in the pathogenesis of chronic myelogenous leukaemia. *Nat. Rev. Cancer.* 5:172–183. https://doi.org/10.1038/nrc1567.
7. Chen, M., A. G. Turhan, …, X. Jiang. 2017. Targeting BCR-ABL+ stem/progenitor cells and BCR-ABL-T315I mutant cells by effective inhibition of the BCR-ABL-Tyr177-GRB2 complex. *Oncotarget.* 8:43662–43677. https://doi.org/10.18632/oncotarget.18216.
8. Mian, A. A., I. Haberbosch, …, J. Mahajna. 2021. Crizotinib acts as ABL1 inhibitor combining ATP-binding with allosteric inhibition and is active against native BCR-ABL1 and its resistance and compound mutants BCR-ABL1(T315I) and BCR-ABL1(T315I-E255K). *Ann. Hematol.* 100:2023–2029. https://doi.org/10.1007/s00277-020-04357-z.
9. Malagrinò, F., A. Coluccia, …, S. Gianni. 2020. Targeting the interaction between the SH3 domain of Grb2 and Gab2. *Cells.* 9:2435. https://doi.org/10.3390/cells9112435.
10. Naughton, R., C. Quiney, …, T. G. Cotter. 2009. Bcr-Abl-mediated redox regulation of the PI3K/AKT pathway. *Leukemia.* 23:1432–1440. https://doi.org/10.1038/leu.2009.49.
11. Lyczek, A., B. T. Berger, …, M. A. Seeliger. 2021. Mutation in Abl kinase with altered drug-binding kinetics indicates a novel mechanism of imatinib resistance. *Proc. Natl. Acad. Sci. U S A.* 118. e2111451118. https://doi.org/10.1073/pnas.2111451118.
12. Million, R. P., and R. A. Van Etten. 2000. The Grb2 binding site is required for the induction of chronic myeloid leukemia-like disease in mice by the Bcr/Abl tyrosine kinase. *Blood.* 96:664–670. https://doi.org/10.1182/blood.v96.2.664.
13. Gregor, T., M. K. Bosakova, …, P. Krejci. 2020. Elucidation of protein interactions necessary for the maintenance of the BCR-ABL signaling complex. *Cell. Mol. Life Sci.* 77:3885–3903. https://doi.org/10.1007/s00018-019-03397-7.
14. Cilloni, D., and G. Saglio. 2012. Molecular pathways: bcr-abl. *Clin. Cancer Res.* 18:930–937. https://doi.org/10.1158/1078-0432.ccr-10-1613.
15. Zhang, M., Z. Luo, …, D. P. Bottaro. 2014. Synergistic anti-leukemic activity of imatinib in combination with a small molecule Grb2 SH2 domain binding antagonist. *Leukemia.* 28:948–951. https://doi.org/10.1038/leu.2013.323.
16. Kanagal-Shamanna, R., C. E. Bueso-Ramos, …, C. C. Yin. 2012. Myeloid neoplasms with isolated isochromosome 17q represent a clinicopathologic entity associated with myelodysplastic/myeloproliferative features, a high risk of leukemic transformation, and wild-type TP53. *Cancer.* 118:2879–2888. https://doi.org/10.1002/cncr.26537.
17. Ohanian, M., A. Tari Ashizawa, …, J. Cortes. 2018. Liposomal Grb2 antisense oligodeoxynucleotide (BP1001) in patients with refractory or relapsed haematological malignancies: a single-centre, open-label, dose-escalation, phase 1/1b trial. *Lancet Haematol.* 5:e136–e146. https://doi.org/10.1016/s2352-3026(18)30021-8.
18. Gishizky, M. L., D. Cortez, and A. M. Pendergast. 1995. Mutant forms of growth factor-binding protein-2 reverse BCR-ABL-induced transformation. *Proc. Natl. Acad. Sci. U S A.* 92:10889–10893. https://doi.org/10.1073/pnas.92.24.10889.
19. Kardinal, C., B. Konkol, …, S. M. Feller. 2001. Chronic myelogenous leukemia blast cell proliferation is inhibited by peptides that disrupt Grb2-SoS complexes. *Blood.* 98:1773–1781. https://doi.org/10.1182/blood.v98.6.1773.

20. Modi, H., L. Li, …, R. Bhatia. 2011. Inhibition of Grb2 expression demonstrates an important role in BCR-ABL-mediated MAPK activation and transformation of primary human hematopoietic cells. *Leukemia.* 25:305–312. https://doi.org/10.1038/leu.2010.257.

21. Chu, S., L. Li, …, R. Bhatia. 2007. BCR-tyrosine 177 plays an essential role in Ras and Akt activation and in human hematopoietic progenitor transformation in chronic myelogenous leukemia. *Cancer Res.* 67:7045–7053. https://doi.org/10.1158/0008-5472.can-06-4312.

22. He, Y., J. A. Wertheim, …, W. S. Pear. 2002. The coiled-coil domain and Tyr177 of bcr are required to induce a murine chronic myelogenous leukemia-like disease by bcr/abl. *Blood.* 99:2957–2968. https://doi.org/10.1182/blood.v99.8.2957.

23. Zhang, X. W., R. Subrahmanyam, …, R. B. Ren. 2001. The NH2-terminal coiled-coil domain and tyrosine 177 play important roles in induction of a myeloproliferative disease in mice by Bcr-Abl. *Mol. Cell Biol.* 21:840–853. https://doi.org/10.1128/mcb.21.3.840-853.2001.

24. Duggal, S., M. K. Midha, …, K. V. Rao. 2019. Outlining the Grb2 interactome data and its interacting partners in HEK293 cells in absence and presence of epidermal growth factor. *Data Brief.* 25:104082. https://doi.org/10.1016/j.dib.2019.104082.

25. Bongartz, H., K. Gille, …, F. Schaper. 2019. The multi-site docking protein Grb2-associated binder 1 (Gab1) enhances interleukin-6-induced MAPK-pathway activation in an SHP2-Grb2-and time-dependent manner. *Cell Commun. Signal.* 17:135. https://doi.org/10.1186/s12964-019-0451-2.

26. Pudewell, S., C. Wittich, …, M. R. Ahmadian. 2021. Accessory proteins of the RAS-MAPK pathway: moving from the side line to the front line. *Commun. Biol.* 4:696. https://doi.org/10.1038/s42003-021-02149-3.

27. Kazemein Jasemi, N. S., C. Herrmann, …, M. R. Ahmadian. 2021. The intramolecular allostery of GRB2 governing its interaction with SOS1 is modulated by phosphotyrosine ligands. *Biochem. J.* 478:2793–2809. https://doi.org/10.1042/bcj20210105.

28. Bolgov, A., S. Korban, …, I. Bezprozvanny. 2020. Crystal structure of the SH3 domain of growth factor receptor-bound protein 2. *Acta. Crystallogr. F Struct. Biol. Commun.* 76:263–270. https://doi.org/10.1107/s2053230x20007232.

29. Rohwedder, A., S. Knipp, …, J. E. Ladbury. 2021. Composition of receptor tyrosine kinase-mediated lipid micro-domains controlled by adaptor protein interaction. *Sci. Rep.* 11:6160. https://doi.org/10.1038/s41598-021-85578-8.

30. Ahmed, Z., Z. Timsah, …, J. E. Ladbury. 2015. Grb2 monomer–dimer equilibrium determines normal versus oncogenic function. *Nat. Commun.* 6:7354. https://doi.org/10.1038/ncomms8354.

31. Xing, F., D. Zhao, …, K. Watabe. 2021. Epigenetic and posttranscriptional modulation of SOS1 can promote breast cancer metastasis through obesity-activated c-met signaling in african-American women. *Cancer Res.* 81:3008–3021. https://doi.org/10.1158/0008-5472.can-19-4031.

32. Qiao, X.-R., X. Zhang, …, Y. Du. 2020. GRB2-associated binding protein 2 regulates multiple pathways associated with the development of prostate cancer. *Oncol. Lett.* 20:1. https://doi.org/10.3892/ol.2020.11960.

33. Dharmawardana, P. G., B. Peruzzi, …, D. P. Bottaro. 2006. Molecular targeting of growth factor receptor-bound 2 (Grb2) as an anti-cancer strategy. *Anti Cancer Drugs.* 17:13–20. https://doi.org/10.1097/01.cad.0000185180.72604.ac.

34. Kessels, H. W. H. G., A. C. Ward, and T. N. M. Schumacher. 2002. Specificity and affinity motifs for Grb2 SH2-ligand interactions. *Proc. Natl. Acad. Sci. U S A.* 99:8524–8529. https://doi.org/10.1073/pnas.142224499.

35. Skolnik, E. Y., C. H. Lee, …, M. F. White. 1993. The SH2/SH3 domain-containing protein GRB2 interacts with tyrosine-phosphorylated IRS1 and Shc: implications for insulin control of ras signalling. *EMBO J.* 12:1929–1936. https://doi.org/10.1002/j.1460-2075.1993.tb05842.x.

36. Rahuel, J., C. García-Echeverría, …, B. Gay. 1998. Structural basis for the high affinity of amino-aromatic SH2 phosphopeptide ligands. *J. Mol. Biol.* 279:1013–1022. https://doi.org/10.1006/jmbi.1998.1790.

37. Dixit, A., and G. M. Verkhivker. 2009. Hierarchical modeling of activation mechanisms in the ABL and EGFR kinase domains: thermodynamic and mechanistic catalysts of kinase activation by cancer mutations. *PLoS Comput. Biol.* 5:e1000487. https://doi.org/10.1371/journal.pcbi.1000487.

38. Rahuel, J., B. Gay, …, M. G. Grütter. 1996. Structural basis for specificity of Grb2-SH2 revealed by a novel ligand binding mode. *Nat. Struct. Biol.* 3:586–589. https://doi.org/10.1038/nsb0796-586.

39. Lin, C. C., L. Wieteska, …, J. E. Ladbury. 2021. Grb2 binding induces phosphorylation-independent activation of Shp2. *Commun. Biol.* 4:437. https://doi.org/10.1038/s42003-021-01969-7.

40. Liao, T. J., H. Jang, …, D. Fushman. 2020. High-affinity interactions of the nSH3/cSH3 domains of Grb2 with the C-terminal proline-rich domain of SOS1. *J. Am. Chem. Soc.* 142:3401–3411. https://doi.org/10.1021/jacs.9b10710.

41. Xiao, T., L. Sun, …, H. Ji. 2021. Synthesis and structural characterization of a monocarboxylic inhibitor for GRB2 SH2 domain. *Bioorg. Med. Chem. Lett.* 51:128354. https://doi.org/10.1016/j.bmcl.2021.128354.

42. Nussinov, R., M. Zhang, …, H. Jang. 2018. Autoinhibition in Ras effectors Raf, PI3Kα, and RASSF5: a comprehensive review underscoring the challenges in pharmacological intervention. *Biophys. Rev.* 10:1263–1282. https://doi.org/10.1007/s12551-018-0461-0.

43. Kharbanda, A., D. M. Walter, …, E. S. Witze. 2020. Blocking EGFR palmitoylation suppresses PI3K signaling and mutant KRAS lung tumorigenesis. *Sci. Signal.* 13:eaax2364. https://doi.org/10.1126/scisignal.aax2364.

44. Roskoski, R., Jr. 2014. The ErbB/HER family of protein-tyrosine kinases and cancer. *Pharmacol. Res.* 79:34–74. https://doi.org/10.1016/j.phrs.2013.11.002.

45. Roskoski, R., Jr. 2021. Blockade of mutant RAS oncogenic signaling with a special emphasis on KRAS. *Pharmacol. Res.* 172:105806. https://doi.org/10.1016/j.phrs.2021.105806.

46. Zhang, M., H. Jang, and R. Nussinov. 2020. PI3K inhibitors: review and new strategies. *Chem. Sci.* 11:5855–5865. https://doi.org/10.1039/d0sc01676d.

47. Liu, B. A., B. W. Engelmann, and P. D. Nash. 2012. The language of SH2 domain interactions defines phosphotyrosine-mediated signal transduction. *FEBS Lett.* 586:2597–2605. https://doi.org/10.1016/j.febslet.2012.04.054.

48. Brooks, B. R., C. L. Brooks, 3rd, …, M. Karplus. 2009. CHARMM: the biomolecular simulation program. *J. Comput. Chem.* 30:1545–1614. https://doi.org/10.1002/jcc.21287.

49. Zhang, M., H. Jang, …, R. Nussinov. 2021. B-Raf autoinhibition in the presence and absence of 14-3-3. *Structure.* 29:768–777.e2. https://doi.org/10.1016/j.str.2021.02.005.

50. Maloney, R. C., M. Zhang, …, R. Nussinov. 2021. The mechanism of activation of monomeric B-Raf V600E. *Comput. Struct. Biotechnol. J.* 19:3349–3363. https://doi.org/10.1016/j.csbj.2021.06.007.

51. Zhang, M., H. Jang, and R. Nussinov. 2019. The mechanism of PI3Kα activation at the atomic level. *Chem. Sci.* 116:341a. https://doi.org/10.1016/j.bpj.2018.11.1858.

52. Jang, H., I. N. Smith, …, R. Nussinov. 2021. The mechanism of full activation of tumor suppressor PTEN at the phosphoinositide-enriched membrane. *iScience.* 24:102438. https://doi.org/10.1016/j.isci.2021.102438.

53. Phillips, J. C., R. Braun, …, K. Schulten. 2005. Scalable molecular dynamics with NAMD. *J. Comput. Chem.* 26:1781–1802. https://doi.org/10.1002/jcc.20289.

54. Huang, J., S. Rauscher, …, A. D. MacKerell, Jr. 2017. CHARMM36m: an improved force field for folded and intrinsically disordered proteins. *Nat. Methods.* 14:71–73. https://doi.org/10.1038/nmeth.4067.

55. Klauda, J. B., R. M. Venable, …, R. W. Pastor. 2010. Update of the CHARMM all-atom additive force field for lipids: validation on six lipid types. *J. Phys. Chem. B.* 114:7830–7843. https://doi.org/10.1021/jp101759q.

56. Baker, N. A., D. Sept, …, J. A. McCammon. 2001. Electrostatics of nanosystems: application to microtubules and the ribosome. *Proc. Natl. Acad. Sci. U S A.* 98:10037–10041. https://doi.org/10.1073/pnas.181342398.

57. Pettersen, E. F., T. D. Goddard, …, T. E. Ferrin. 2004. UCSF chimera - a visualization system for exploratory research and analysis. *J. Comput. Chem.* 25:1605–1612. https://doi.org/10.1002/jcc.20084.

58. Weako, J., H. Jang, …, A. Gursoy. 2021. The structural basis of Akt PH domain interaction with calmodulin. *Biophys. J.* 120:1994–2008. https://doi.org/10.1016/j.bpj.2021.03.018.

59. Jang, H., A. Banerjee, …, R. Nussinov. 2019. The structural basis of the farnesylated and methylated KRas4B interaction with calmodulin. *Structure.* 27:1647–1659.e4. https://doi.org/10.1016/j.str.2019.08.009.

60. Liao, T.-J., H. Jang, D. Fushman, and R. Nussinov. 2018. Allosteric KRas4B can modulate SOS1 fast and slow Ras activation cycles. *Biophys. J.* 115:629–641. https://doi.org/10.1016/j.bpj.2018.07.016.

61. Ozdemir, E. S., H. Jang, …, R. Nussinov. 2018. Unraveling the molecular mechanism of interactions of the Rho GTPases Cdc42 and Rac1 with the scaffolding protein IQGAP2. *J. Biol. Chem.* 293:3685–3699. https://doi.org/10.1074/jbc.ra117.001596.

62. Jang, H., A. Banerjee, …, R. Nussinov. 2017. Flexible-body motions of calmodulin and the farnesylated hypervariable region yield a high-affinity interaction enabling K-Ras4B membrane extraction. *J. Biol. Chem.* 292:12544–12559. https://doi.org/10.1074/jbc.m117.785063.

63. Zhang, M., H. Jang, …, R. Nussinov. 2017. Phosphorylated calmodulin promotes PI3K activation by binding to the SH2 domains. *Biophys. J.* 113:1956–1967. https://doi.org/10.1016/j.bpj.2017.09.008.

64. Jang, H., S. Muratcioglu, …, R. Nussinov. 2016. Membrane-associated Ras dimers are isoform-specific: K-Ras dimers differ from H-Ras dimers. *Biochem. J.* 473:1719–1732. https://doi.org/10.1042/bcj20160031.

65. Im, W., M. S. Lee, and C. L. Brooks, 3rd. 2003. Generalized born model with a simple smoothing function. *J. Comput. Chem.* 24:1691–1702. https://doi.org/10.1002/jcc.10321.

66. Liu, B. A., K. Jablonowski, …, P. D. Nash. 2006. The human and mouse complement of SH2 domain proteins-establishing the boundaries of phosphotyrosine signaling. *Mol. Cell.* 22:851–868. https://doi.org/10.1016/j.molcel.2006.06.001.

67. Dai, K., S. Liao, …, X. Tu. 2011. Solution structure of tensin2 SH2 domain and its phosphotyrosine-independent interaction with DLC-1. *PLoS One.* 6:e21965. https://doi.org/10.1371/journal.pone.0021965.

68. Liao, Y. C., L. Si, …, S. H. Lo. 2007. The phosphotyrosine-independent interaction of DLC-1 and the SH2 domain of cten regulates focal adhesion localization and growth suppression activity of DLC-1. *J. Cell Biol.* 176:43–49. https://doi.org/10.1083/jcb.200608015.

69. Huang, H., L. Li, …, S. S. C. Li. 2008. Defining the specificity space of the human SRC homology 2 domain. *Mol. Cell. Proteomics.* 7:768–784. https://doi.org/10.1074/mcp.m700312-mcp200.

70. Sanches, K., I. P. Caruso, …, F. A. Melo. 2020. The dynamics of free and phosphopeptide-bound Grb2-SH2 reveals two dynamically independent subdomains and an encounter complex with fuzzy interactions. *Sci. Rep.* 10:13040. https://doi.org/10.1038/s41598-020-70034-w.

71. Liu, B. A., B. W. Engelmann, and P. D. Nash. 2012. High-throughput analysis of peptide-binding modules. *Proteomics.* 12:1527–1546. https://doi.org/10.1002/pmic.201100599.

72. Zhang, M., Z. Li, …, R. Nussinov. 2018. Calmodulin (CaM) activates PI3Kα by targeting the "soft" CaM-binding motifs in both the nSH2 and cSH2 domains of p85α. *J. Phys. Chem. B.* 122:11137–11146. https://doi.org/10.1021/acs.jpcb.8b05982.

73. Wilmot, C. M., and J. M. Thornton. 1988. Analysis and prediction of the different types of beta-turn in proteins. *J. Mol. Biol.* 203:221–232. https://doi.org/10.1016/0022-2836(88)90103-9.

74. Songyang, Z., S. E. Shoelson, …, T. Yi. 1994. Specific motifs recognized by the SH2 domains of Csk, 3BP2, fps/fes, GRB-2, HCP, SHC, Syk, and Vav. *Mol. Cell Biol.* 14:2777–2785. https://doi.org/10.1128/mcb.14.4.2777-2785.1994.

75. Mohanty, P., and S. Bhatnagar. 2017. Structural basis of focal adhesion targeting domain-mediated signaling in cardiac hypertrophy. *J. Recept. Signal Transduct. Res.* 37 (1):38–50. https://doi.org/10.3109/10799893.2016.1155067.

76. Nagar, B., O. Hantschel, …, J. Kuriyan. 2003. Structural basis for the autoinhibition of c-Abl tyrosine kinase. *Cell.* 112:859–871. https://doi.org/10.1016/s0092-8674(03)00194-6.

77. Xie, T., T. Saleh, …, C. G. Kalodimos. 2020. Conformational states dynamically populated by a kinase determine its function. *Science.* 370:eabc2754. https://doi.org/10.1126/science.abc2754.

78. Kraskouskaya, D., E. Duodu, …, P. T. Gunning. 2013. Progress towards the development of SH2 domain inhibitors. *Chem. Soc. Rev.* 42:3337. https://doi.org/10.1039/c3cs35449k.

79. Nioche, P., W. Q. Liu, …, A. Ducruix. 2002. Crystal structures of the SH2 domain of Grb2: highlight on the binding of a new high-affinity inhibitor. *J. Mol. Biol.* 315:1167–1177. https://doi.org/10.1006/jmbi.2001.5299.

80. Machida, K., and B. J. Mayer. 2005. The SH2 domain: versatile signaling module and pharmaceutical target. *Biochim. Biophys. Acta.* 1747:1–25. https://doi.org/10.1016/j.bbapap.2004.10.005.

Biophysical Journal, Volume *121*

Supplemental information

The structural basis of BCR-ABL recruitment of GRB2 in chronic myelogenous leukemia

Yonglan Liu, Hyunbum Jang, Mingzhen Zhang, Chung-Jung Tsai, Ryan Maloney, and Ruth Nussinov

The structural basis of BCR-ABL recruitment of GRB2 in chronic myelogenous leukemia

Yonglan Liu[a], Hyunbum Jang[b], Mingzhen Zhang[b], Chung-Jung Tsai[b], Ryan Maloney[a] and Ruth Nussinov[b,c,*]

[a]Computational Structural Biology Section, Cancer Innovation Laboratory, National Cancer Institute, Frederick, MD 21702, U.S.A.

[b]Computational Structural Biology Section, Cancer Innovation Laboratory, Frederick National Laboratory for Cancer Research, Frederick, MD 21702, U.S.A.

[c]Department of Human Molecular Genetics and Biochemistry, Sackler School of Medicine, Tel Aviv University, Tel Aviv 69978, Israel

Author for correspondence:

Tel: 301-846-5579

E-mail: NussinoR@mail.nih.gov

The authors declare no potential conflicts of interest.

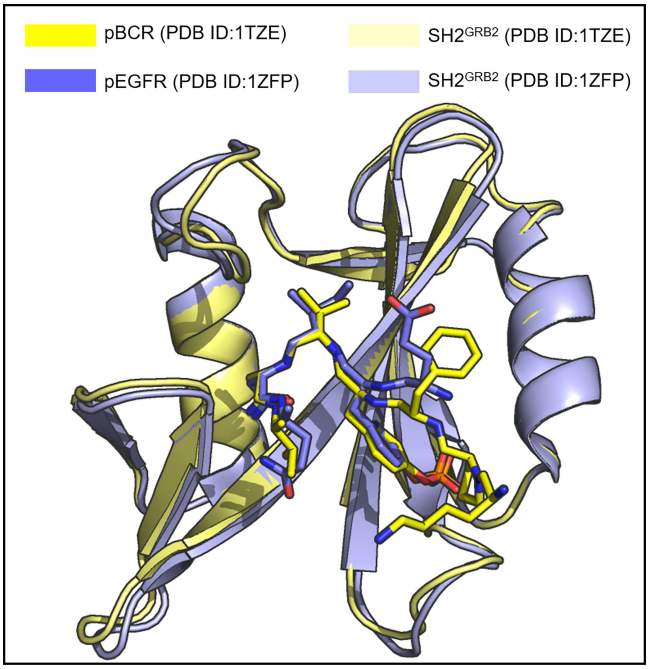

Figure S1. Superimposition of the conformations from the two different crystal structures of $SH2^{GRB2}$ in complex with pBCR ($_{174}$KPFpYVNV$_{180}$) (PDB ID: 1TZE) and pEGFR ($_{1067}$EpYINQ$_{1071}$) (PDB ID: 1ZFP) peptides. $SH2^{GRB2}$ shown as cartoon is colored light yellow and light blue in complex with pBCR and pEGFR, respectively. Both pBCR and pEGFR peptides shown as sticks are colored yellow and blue, respectively.

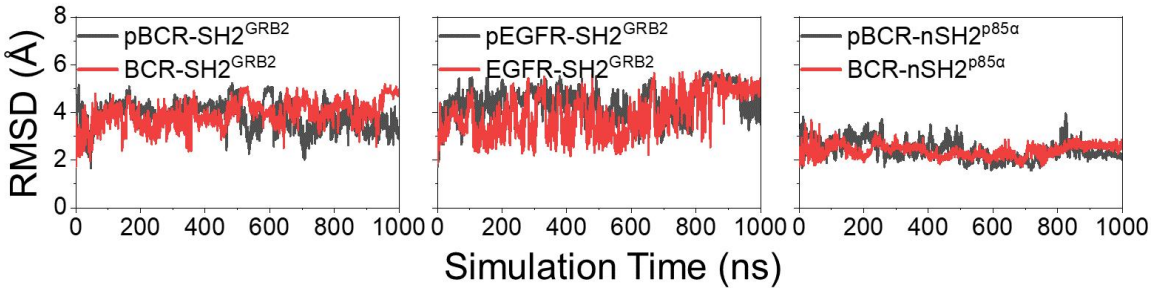

Figure S2. Time evolution of root-mean-square deviations (RMSDs) for pBCR–$SH2^{GRB2}$ and BCR–$SH2^{GRB2}$, pEGFR–$SH2^{GRB2}$ and EGFR–$SH2^{GRB2}$, and pBCR–$nSH2^{p85\alpha}$ and BCR–$nSH2^{p85\alpha}$.

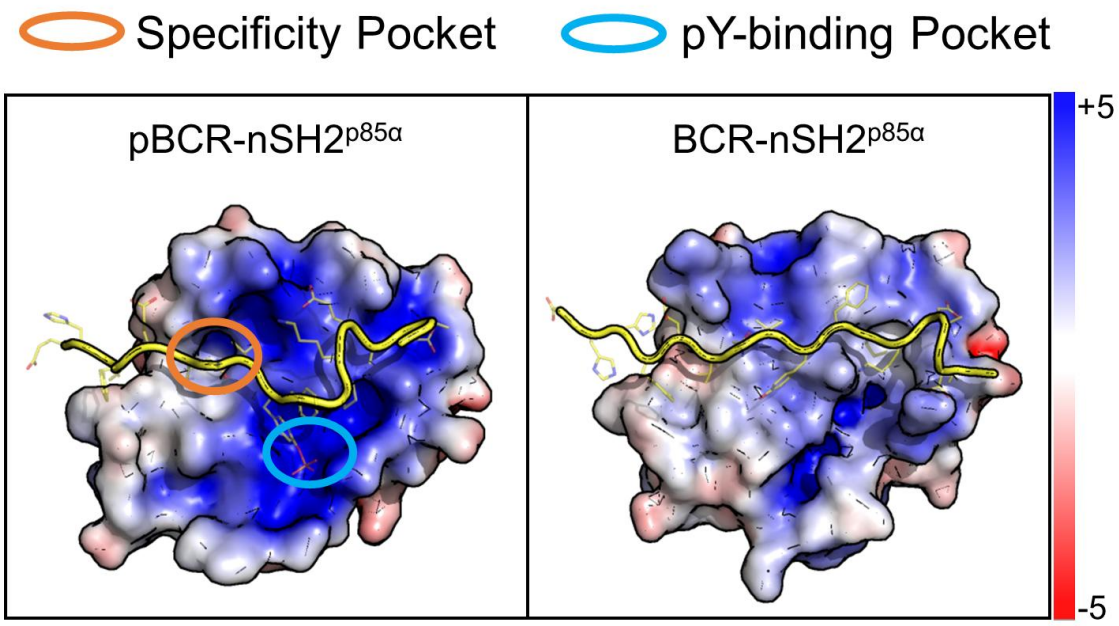

Figure S3. Binding modes of pBCR–nSH2$^{p85\alpha}$ and BCR–nSH2$^{p85\alpha}$ systems. nSH2$^{p85\alpha}$ shown as electrostatic surface is colored based on the charge properties (red, negative charge; blue, positive charge), characterizing the electrostatic surfaces of nSH2$^{p85\alpha}$. The peptides shown as tubes are colored yellow. The cartoon structures of protein represent the averaged structures over the last half of the simulations. The representative structures account for 63.6% and 60.8 % of the ensemble structures over the last half of the trajectories for pBCR–nSH2$^{p85\alpha}$ and BCR–nSH2$^{p85\alpha}$, respectively.

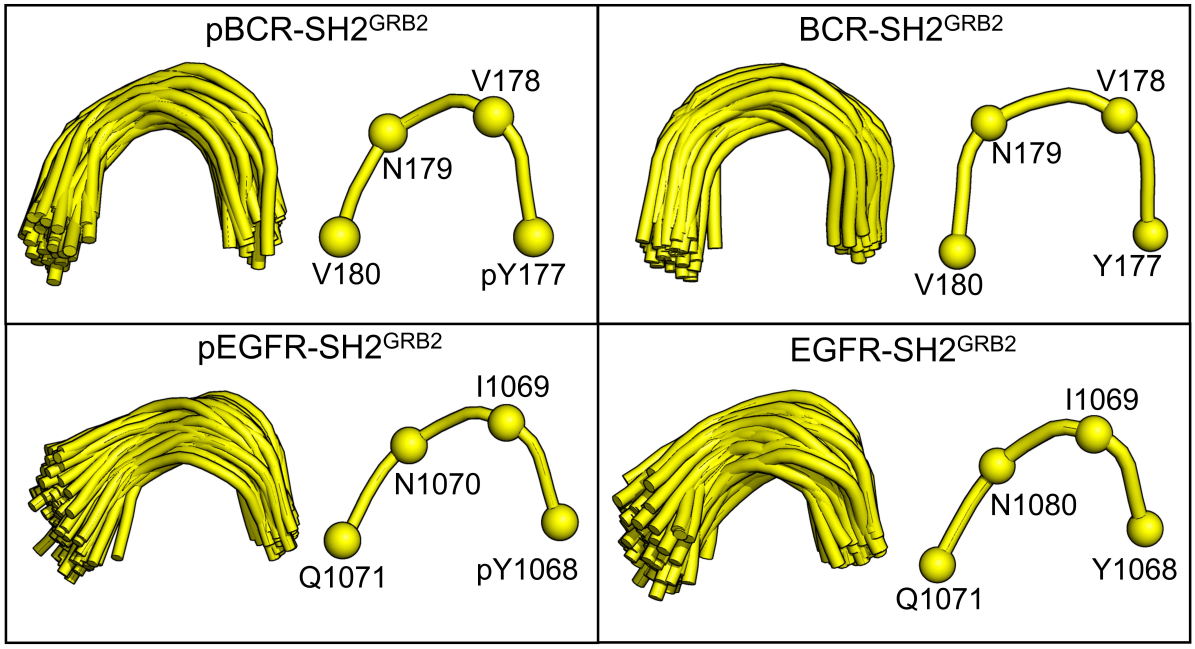

Figure S4. Structural alignment (left) of the type I β-turn region (residues from the pY position to the +3 position C-terminal to pY) and the representative conformation of type I β-turn (right) for each peptide in the bound state for the pBCR-SH2^{GRB2}, BCR-SH2^{GRB2}, pEGFR-SH2^{GRB2}, and EGFR-SH2^{GRB2} systems. In the cartoons, the peptides are shown as tubes. In the representative conformations, spheres denote the Cα atoms of β-turn residues. These residues are marked on each peptide. Superimpositions of the aligned structures were obtained from the last half of the simulations.

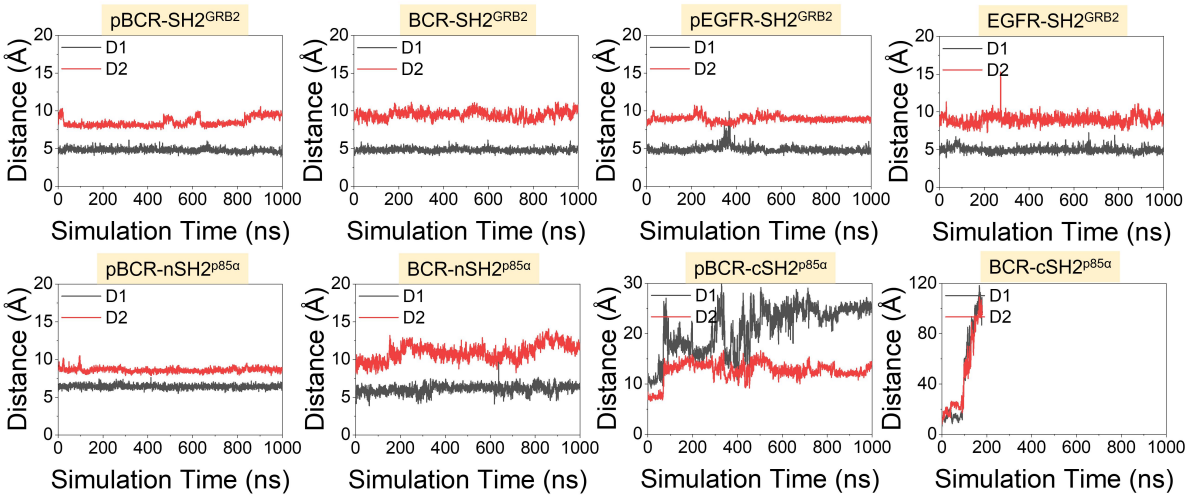

Figure S5. Time evolution of D1 and D2 for pBCR–SH2^{GRB2} and BCR–SH2^{GRB2}, pEGFR–SH2^{GRB2} and EGFR–SH2^{GRB2}, and pBCR–nSH2$^{p85\alpha}$ and BCR–nSH2$^{p85\alpha}$, and pBCR–cSH2$^{p85\alpha}$ and BCR–cSH2$^{p85\alpha}$. D1 is the distance between the Cα atom of N179 in pBCR/BCR, or N1070 in pEGFR/EGFR, and the center of mass of the Cα atoms of the residues (F108, K109, L120, and W121 in SH2^{GRB2}; I381, F392, Y416, and N417 in nSH2$^{p85\alpha}$; and C670, F681, H706, and L710 in cSH2$^{p85\alpha}$) forming the specificity pocket of the SH2 domains. D2 is the distance between the Cα atom of pY177 in pBCR, Y177 in BCR, pY1068 in pEGFR, or Y1068 in EGFR, and the Cα atoms of the residues (R67, R86, S88, S90, S96, H107, and K109 in SH2^{GRB2}; R340, R358, S361, T362, K382, and L380 in nSH2$^{p85\alpha}$; and R631, R639, H669, and V671 in cSH2$^{p85\alpha}$) forming the pY-binding pocket of the SH2 domains.

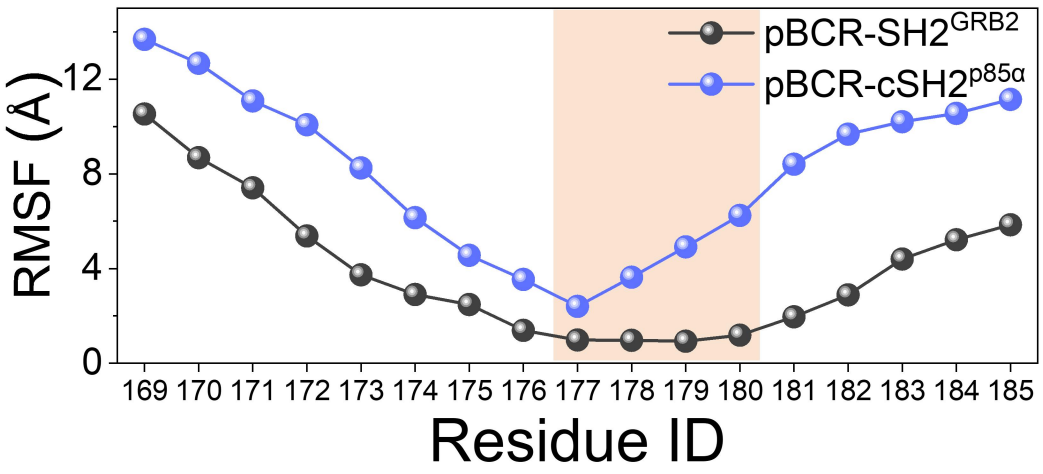

Figure S6. Root-mean-square fluctuations (RMSFs) of pBCR in the pBCR-SH2^{GRB2} and pBCR-cSH2$^{p85\alpha}$ systems. RMSFs are calculated for the last half of the simulations.

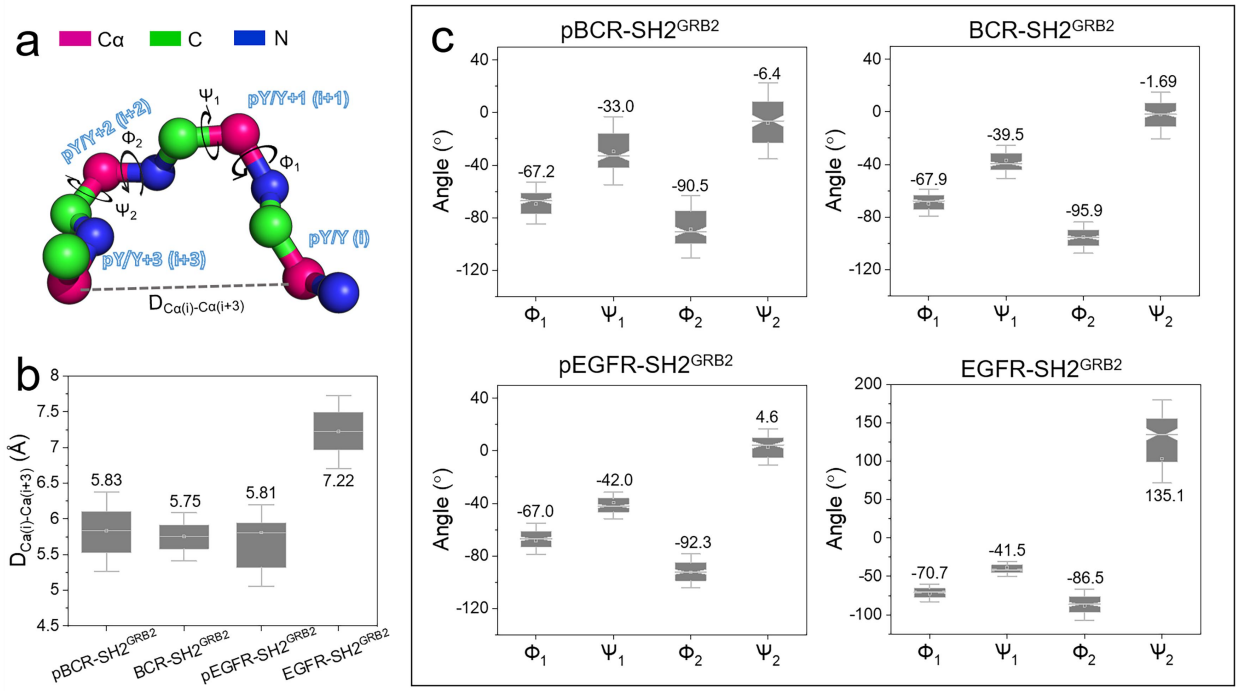

Figure S7. Characterization of type I β-turn conformation of pY/Y-peptides in complex with $SH2^{GRB2}$. (a) Definition of $D_{Cα(i)-Cα(i+3)}$ and the torsion angles of ϕ_1, ψ_1, ϕ_2, and ψ_2. (b) $D_{Cα(i)-Cα(i+3)}$ and (c) ϕ_1, ψ_1, ϕ_2, and ψ_2 of the peptides in pBCR–$SH2^{GRB2}$, BCR–$SH2^{GRB2}$, pEGFR–$SH2^{GRB2}$, and EGFR–$SH2^{GRB2}$.

a

Affinity order	0	1	2	3
1	pY	V	N	I
2	pY	E	N	V
3	pY	V	N	V
4	pY	K	N	I
5	pY	V	N	Q
6	pY	Q	N	L
6	pY	I	N	A
8	pY	K	N	L
8	pY	M	N	M
10	pY	I	N	Q

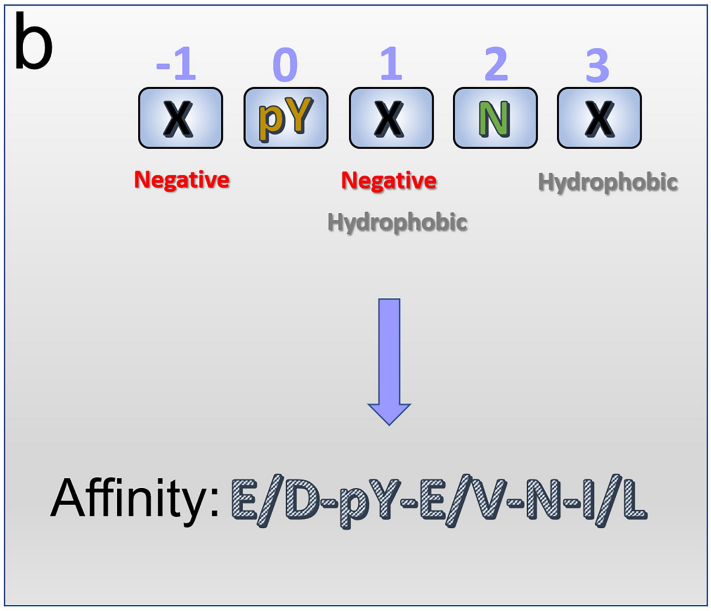

Figure S8. (a) $SH2^{GRB2}$-binding motifs collected from literatures. The motifs are sorted in the decreasing order of binding affinity to $SH2^{GRB2}$. (b) Putative five-residue motifs for the binding of $SH2^{GRB2}$ with the optimal binding affinity.

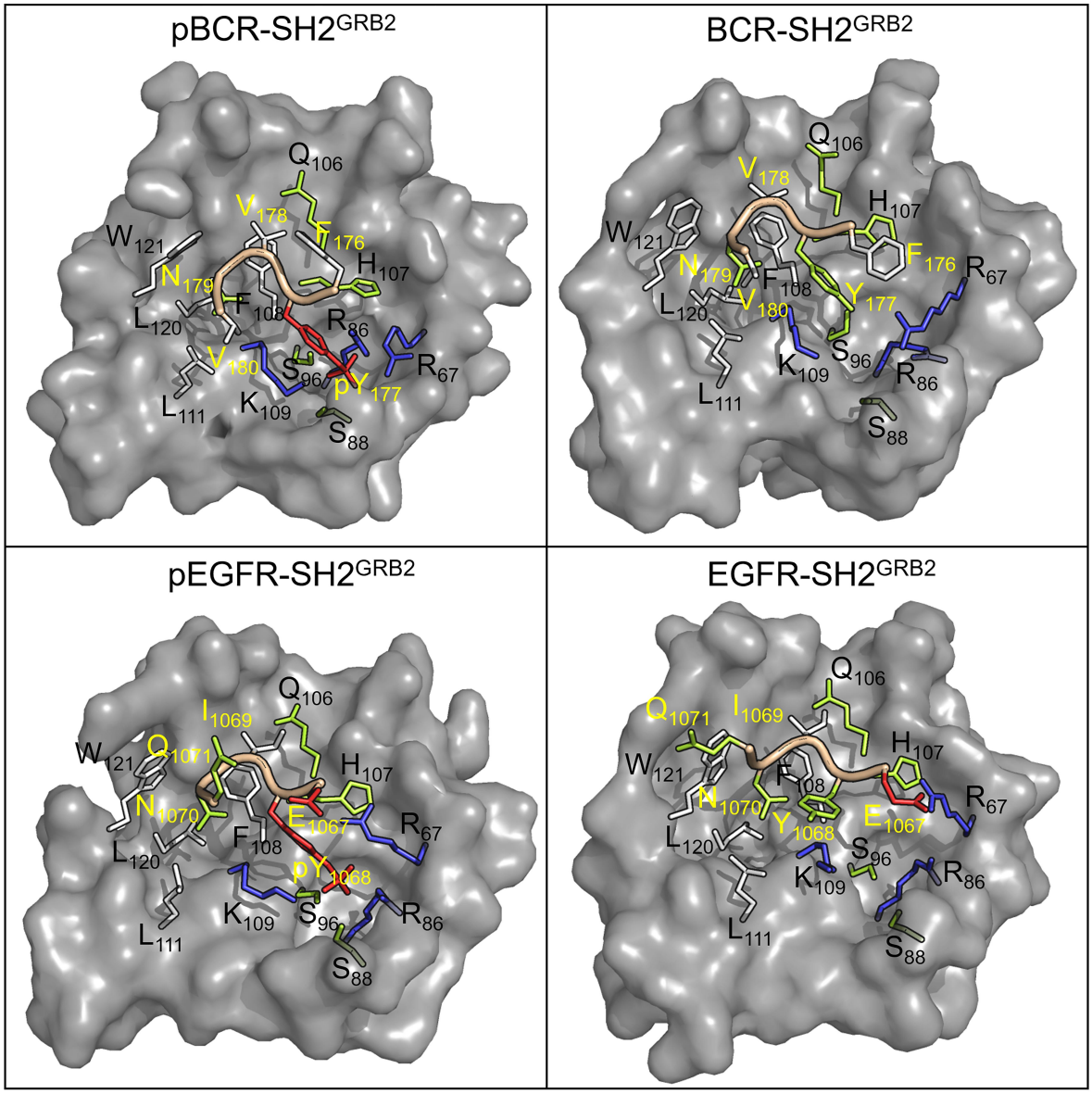

Figure S9. Interaction interfaces of pBCR–SH2^{GRB2}, BCR–SH2^{GRB2}, pEGFR–SH2^{GRB2}, and EGFR–SH2^{GRB2} systems. Interfacial residues are shown as sticks. Hydrophobic, hydrophilic, positively charged, and negatively charged residues are colored white, green, blue, and red, respectively. The yellow and black labels denote the peptide and SH2^{GRB2} residues, respectively.

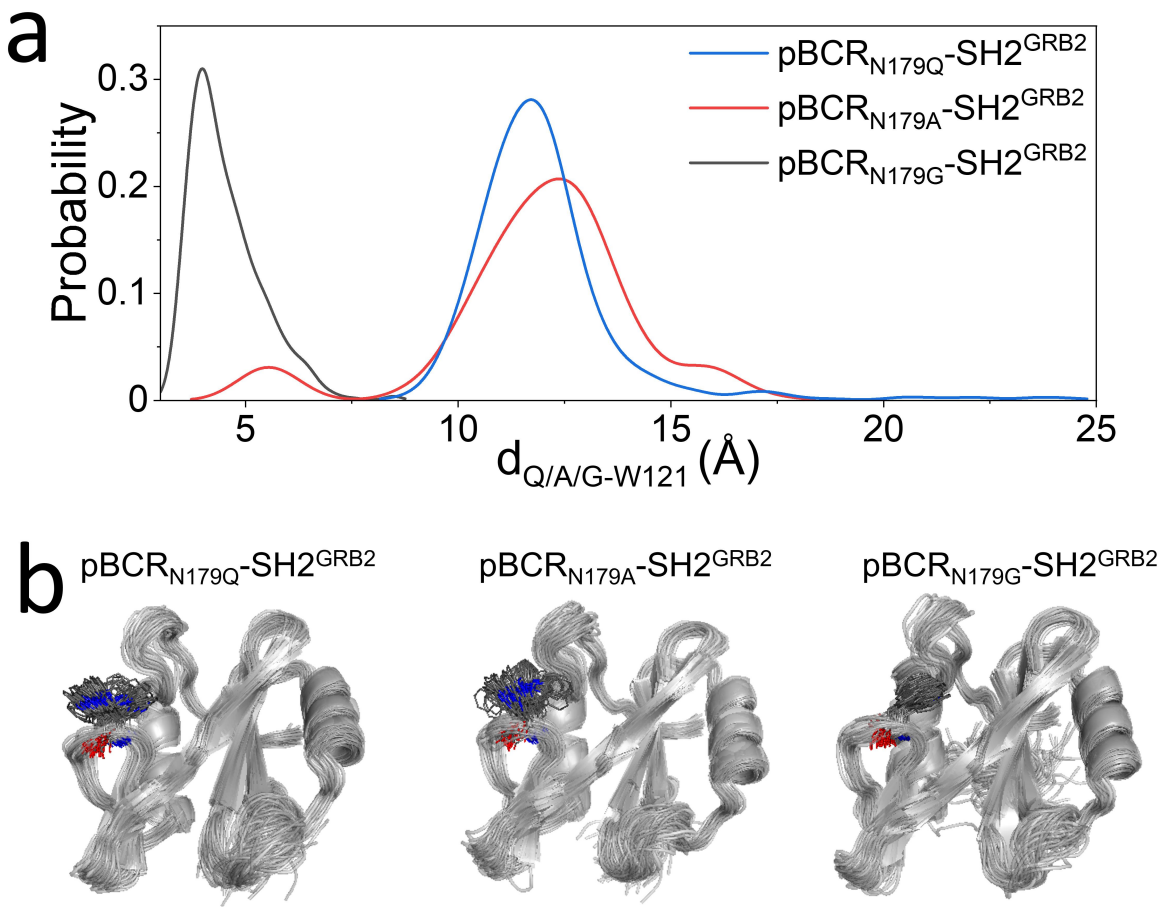

Figure S10. (a) Probability distribution functions of the distance between W121 in $SH2^{GRB2}$ and Q179/A179/G179 in $pBCR_{N179Q}$/$pBCR_{N179A}$/$pBCR_{N179G}$, $d_{Q/A/G-W121}$, and (b) superimposed snapshots representing the dynamic behaviors of W121 sidechain for $pBCR_{N179Q}$–$SH2^{GRB2}$, $pBCR_{N179A}$–$SH2^{GRB2}$, and $pBCR_{N179G}$–$SH2^{GRB2}$.

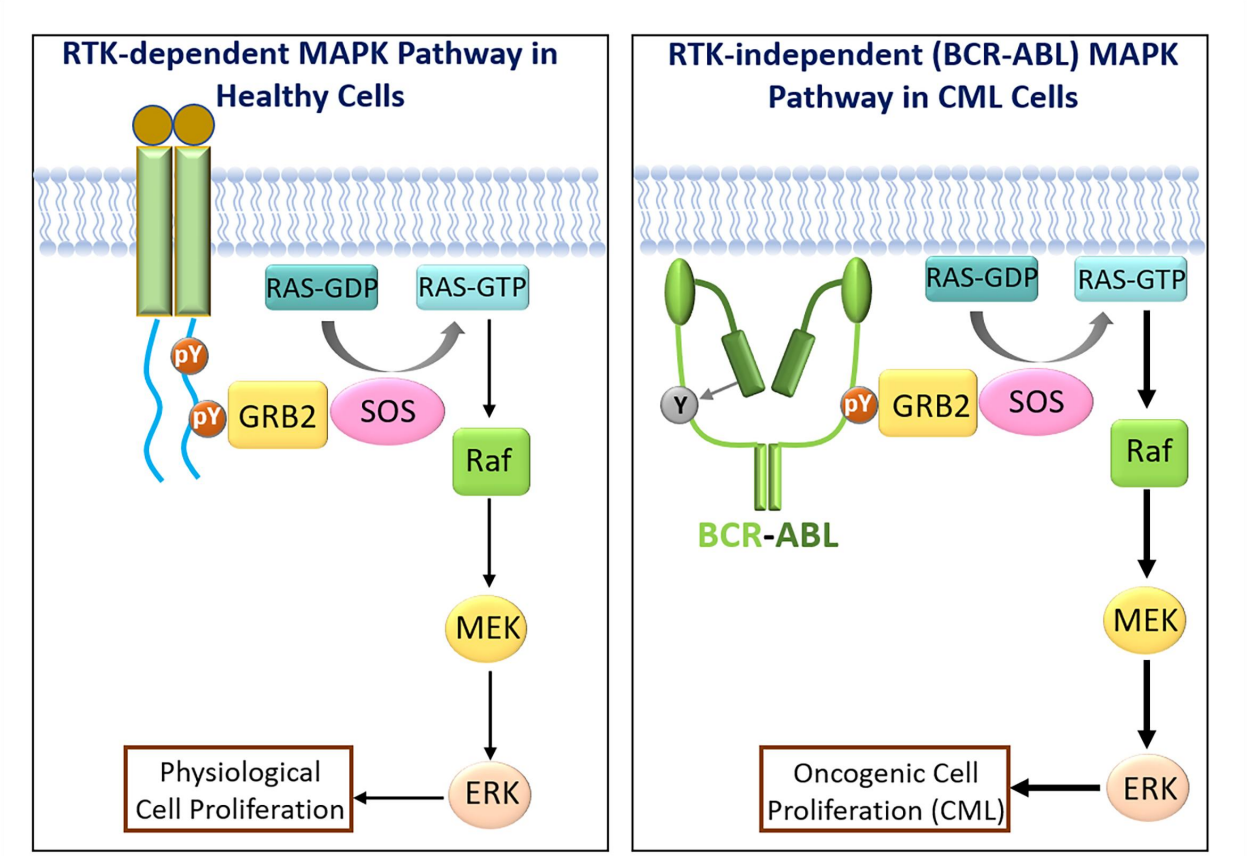

Figure S11. Schematic illustration of RTK-dependent in healthy cells and BCR-ABL-dependent Ras/MAPK signaling pathways in CML cells.

Table S1. Intermolecular pair residues with contact probability >=60% for pY/Y–SH2^{GRB2} systems.

pBCR-SH2^{GRB2}	BCR-SH2^{GRB2}	pEGFR-SH2^{GRB2}	EGFR-SH2^{GRB2}
F176-H107	F176-R67	E1067-R67	E1067-H107
pY177-R67	F176-H107	E1067-H107	Y1068-S96
pY177-R86	Y177-S96	pY1068-R67	Y1068-H107
pY177-S88	Y177-H107	pY1068-R86	Y1068-F108
pY177-S96	Y177-F108	pY1068-S88	Y1068-K109
pY177-H107	Y177-K109	pY1068-S96	I1069-Q106
pY177-F108	V178-Q106	pY1068-H107	I1069-H107
pY177-K109	V178-H107	pY1068-F108	I1069-F108
V178-Q106	V178-F108	pY1068-K109	I1069-W121
V178-H107	V178-W121	I1069-Q106	I1069-S141
V178-F108	V178-S141	I1069-H107	N1070-F108
N179-F108	N179-F108	I1069-F108	N1070-K109
N179-K109	N179-K109	I1069-W121	N1070-L111
N179-L111	N179-L111	N1070-F108	N1070-L120
N179-L120	N179-L120	N1070-K109	N1070-W121
N179-W121	N179-W121	N1070-L111	
V180-K109	V180-K109	N1070-L120	
V180-L111	V180-L111	N1070-W121	
F182-W121	E185-R67		
E185-R142			

Table S2. pY-peptides of different proteins with affinity to the $SH2^{GRB2}$ domain.

Protein Name	pTyr Peptide Sequence	Reference
BCR	$_{174}$KPFpYVNV$_{180}$	(1)
EGFR	$_{1067}$EpYINQ$_{1071}$	(2)
β-PDGFR	$_{701}$LQHHSDKRRPPSAELpYSNALPVG$_{723}$	(3)
DF3	$_{1243}$pYTNP$_{1246}$	(4)
SIT	$_{90}$pYGNL$_{93}$	(5)
SIT	$_{188}$pYANS$_{191}$	(5)
IRS-1	$_{891}$SPGEpYVNIEFGS$_{902}$	(6)
SHC	$_{314}$DPSpYVNVNQNL$_{324}$	(6)
SHC	$_{236}$DHQpYYND$_{242}$	(7)
SHP2	$_{542}$pYTNI$_{545}$	(8)
SHP2	$_{584}$pYENV$_{587}$	(9)
FAK	$_{924}$VpYENV$_{928}$	(10)
c-MET	$_{1356}$pYVNV$_{1359}$	(11)
c-Kit/SCFR	$_{694}$QEDHAEAALpYKNLLHSKESS$_{713}$	(12)
c-Kit/SCFR	$_{928}$ISESTNHIpYSNLANCSPNR$_{946}$	(12)
CD28	$_{188}$HSDpYMNMTPR$_{197}$	(13,14)
AICD	$_{679}$QNGpYENPTY$_{687}$	(15)
Modified AICD	$_{679}$QNGpYVNPTY$_{687}$	(15)
LAT	$_{108}$ASpYENE$_{113}$	(16)
LAT	$_{125}$DDpYHNP$_{130}$	(16)
LAT	$_{169}$DDpYVNV$_{174}$	(16)

LAT	$_{189}$REpYVNV$_{194}$	(16)
LAT	$_{224}$PDpYENL$_{229}$	(16)
PLD2	$_{168}$NpYLNR$_{172}$	(17)
PLD2	$_{178}$FpYRNY$_{182}$	(17)
HER2/Neu	$_{1138}$EpYVNQ$_{1142}$	(18)

Table S3. Intermolecular pair residues with interaction energies <-20 kcal/mol for pY/Y-peptide–SH2^{GRB2} systems.

pBCR–SH2^{GRB2}	Energy (kcal/mol)	BCR–SH2^{GRB2}	Energy (kcal/mol)	pEGFR–SH2^{GRB2}	Energy (kcal/mol)	EGFR–SH2^{GRB2}	Energy (kcal/mol)
pY177-R67	-138.35±3.85	E185-R67	-63.64±20.64	pY1068-R67	-128.26±4.64	E1067-R67	-40.59±4.90
pY177-R86	-127.18±2.66	E185-R86	-29.01±7.12	pY1068-R86	-95.83±5.23		
pY177-K109	-144.68±5.61	E185-K109	-59.05±17.37	pY1068-K109	-154.9±8.45		
pY177-S88	-27.29±3.31			pY1068-S88	-29.73±2.33		
pY177-S90	-26.11±2.58			E1067-R67	-49.14±3.48		
pY177-S96	-28.51±2.79						
E185-R142	-78.82±15.89						

Table S4. Hydrogen bonds between residues in $SH2^{GRB2}$ domain and residues in pBCR, BCR, pEGFR, and EGFR.

System	Donor	Acceptor	Occupancy (%)
pBCR–$SH2^{GRB2}$	$R67^{GRB2}$-S	$pY177^{pBCR}$-S	100.00
	$R86^{GRB2}$-S	$pY177^{pBCR}$-S	100.00
	$S88^{GRB2}$-S	$pY177^{pBCR}$-S	69.36
	$S90^{GRB2}$-S	$pY177^{pBCR}$-S	54.80
	$S96^{GRB2}$-S	$pY177^{pBCR}$-S	99.04
	$K109^{GRB2}$-S	$pY177^{pBCR}$-S	90.56
	$V178^{pBCR}$-B	$H107^{GRB2}$-B	92.56
	$K109^{GRB2}$-B	$N179^{pBCR}$-S	95.60
	$N179^{pBCR}$-S	$K109^{GRB2}$-B	97.60
	$N179^{pBCR}$-S	$L120^{GRB2}$-B	86.08
BCR–$SH2^{GRB2}$	$V178^{BCR}$-B	$H107^{GRB2}$-B	91.60
	$N179^{BCR}$-S	$K109^{GRB2}$-B	97.12
	$K109^{GRB2}$-B	$N179^{BCR}$-S	94.40
	$N179^{BCR}$-S	$L120^{GRB2}$-B	86.40
	$R67^{GRB2}$-S	$E185^{BCR}$-S	59.36
pEGFR–$SH2^{GRB2}$	$R67^{GRB2}$-S	$pY1068^{pEGFR}$-S	98.40
	$R86^{GRB2}$-S	$pY1068^{pEGFR}$-S	85.04
	$S88^{GRB2}$-S	$pY1068^{pEGFR}$-S	93.52
	$S96^{GRB2}$-S	$pY1068^{pEGFR}$-S	82.40
	$K109^{GRB2}$-S	$pY1068^{pEGFR}$-S	98.64

	I1069^{pEGFR}-B	H107^{GRB2}-B	87.44
	N1070^{pEGFR}-S	K109^{GRB2}-B	97.44
	K109^{GRB2}-B	N1070^{pEGFR}-S	97.44
	N1070^{pEGFR}-S	L120^{GRB2}-B	85.76
EGFR–SH2^{GRB2}	I1069^{EGFR}-B	H107^{GRB2}-B	86.64
	K109^{GRB2}-B	N1070^{EGFR}-S	94.56
	N1070^{EGFR}-S	K109^{GRB2}-B	89.28
	N1070^{EGFR}-S	L120^{GRB2}-B	76.24

Hydrogen bonds listed in the table have the occupancy > 50% during last 500-ns simulations. S and B indicate sidechain and backbone of residues.

References

1. Rahuel, J., B. Gay, D. Erdmann, A. Strauss, C. Garcia-Echeverria, P. Furet, G. Caravatti, H. Fretz, J. Schoepfer, and M. G. Grutter. 1996. Structural basis for specificity of Grb2-SH2 revealed by a novel ligand binding mode. *Nat Struct Biol*. 3(7):586-589.
2. Rahuel, J., C. Garcia-Echeverria, P. Furet, A. Strauss, G. Caravatti, H. Fretz, J. Schoepfer, and B. Gay. 1998. Structural basis for the high affinity of amino-aromatic SH2 phosphopeptide ligands. *J Mol Biol*. 279(4):1013-1022.
3. Arvidsson, A. K., E. Rupp, E. Nanberg, J. Downward, L. Ronnstrand, S. Wennstrom, J. Schlessinger, C. H. Heldin, and L. Claessonwelsh. 1994. Tyr-716 in the Platelet-Derived Growth-Factor Beta-Receptor Kinase Insert Is Involved in Grb2 Binding and Ras Activation. *Molecular and Cellular Biology*. 14(10):6715-6726.
4. Pandey, P., S. Kharbanda, and D. Kufe. 1995. Association of the DF3/MUC1 breast cancer antigen with Grb2 and the Sos/Ras exchange protein. *Cancer Res*. 55(18):4000-4003.
5. Pfrepper, K. I., A. Marie-Cardine, L. Simeoni, Y. Kuramitsu, A. Leo, J. Spicka, I. Hilgert, J. Scherer, and B. Schraven. 2001. Structural and functional dissection of the cytoplasmic domain of the transmembrane adaptor protein SIT (SHP2-interacting transmembrane adaptor protein). *Eur J Immunol*. 31(6):1825-1836.
6. Skolnik, E. Y., C. H. Lee, A. Batzer, L. M. Vicentini, M. Zhou, R. Daly, M. J. Myers, Jr., J. M. Backer, A. Ullrich, M. F. White, and et al. 1993. The SH2/SH3 domain-containing protein GRB2 interacts with tyrosine-phosphorylated IRS1 and Shc: implications for insulin control of ras signalling. *EMBO J*. 12(5):1929-1936.
7. Harmer, S. L., and A. L. DeFranco. 1997. Shc contains two Grb2 binding sites needed for efficient formation of complexes with SOS in B lymphocytes. *Mol Cell Biol*. 17(7):4087-4095.
8. Bennett, A. M., T. L. Tang, S. Sugimoto, C. T. Walsh, and B. G. Neel. 1994. Protein-tyrosine-phosphatase SHPTP2 couples platelet-derived growth factor receptor beta to Ras. *Proc Natl Acad Sci U S A*. 91(15):7335-7339.
9. Vogel, W., and A. Ullrich. 1996. Multiple in vivo phosphorylated tyrosine phosphatase SHP-2 engages binding to Grb2 via tyrosine 584. *Cell Growth Differ*. 7(12):1589-1597.
10. Schlaepfer, D. D., S. K. Hanks, T. Hunter, and P. van der Geer. 1994. Integrin-mediated signal transduction linked to Ras pathway by GRB2 binding to focal adhesion kinase. *Nature*. 372(6508):786-791.
11. Schiering, N., E. Casale, P. Caccia, P. Giordano, and C. Battistini. 2000. Dimer formation through domain swapping in the crystal structure of the Grb2-SH2-Ac-pYVNV complex. *Biochemistry*. 39(44):13376-13382.
12. Thömmes, K., J. Lennartsson, M. CARLBERG, and L. Rönnstrand. 1999. Identification of Tyr-703 and Tyr-936 as the primary association sites for Grb2 and Grb7 in the c-Kit/stem cell factor receptor. *Biochemical Journal*. 341(1):211-216.
13. Higo, K., T. Ikura, M. Oda, H. Morii, J. Takahashi, R. Abe, and N. Ito. 2013. High resolution crystal structure of the Grb2 SH2 domain with a phosphopeptide derived from CD28. *PLoS One*. 8(9):e74482.
14. Schneider, H., Y. C. Cai, K. V. Prasad, S. E. Shoelson, and C. E. Rudd. 1995. T cell antigen CD28 binds to the GRB-2/SOS complex, regulators of p21ras. *Eur J Immunol*. 25(4):1044-1050.
15. Das, S., M. Raychaudhuri, U. Sen, and D. Mukhopadhyay. 2011. Functional Implications of the Conformational Switch in AICD Peptide upon Binding to Grb2-SH2 Domain. *Journal of Molecular Biology*. 414(2):217-230.

16. Cho, S., C. A. Velikovsky, C. P. Swaminathan, J. C. Houtman, L. E. Samelson, and R. A. Mariuzza. 2004. Structural basis for differential recognition of tyrosine-phosphorylated sites in the linker for activation of T cells (LAT) by the adaptor Gads. *EMBO J*. 23(7):1441-1451.
17. Di Fulvio, M., N. Lehman, X. Lin, I. Lopez, and J. Gomez-Cambronero. 2006. The elucidation of novel SH2 binding sites on PLD2. *Oncogene*. 25(21):3032-3040.
18. Dankort, D., N. Jeyabalan, N. Jones, D. J. Dumont, and W. J. Muller. 2001. Multiple ErbB-2/Neu phosphorylation sites mediate transformation through distinct effector proteins. *Journal of Biological Chemistry*. 276(42):38921-38928.